Article

Triassic diapsid shows early diversification of skin appendages in reptiles

https://doi.org/10.1038/s41586-025-09167-9

Received: 24 September 2024

Accepted: 15 May 2025

Published online: 23 July 2025

Open access

Check for updates

Stephan N. F. Spiekman[1]✉, Christian Foth[2,3,4], Valentina Rossi[5,6], Cristina Gascó Martín[1], Tiffany S. Slater[5,6], Orla G. Bath Enright[1,7], Kathleen N. Dollman[8], Giovanni Serafini[9], Dieter Seegis[1], Léa Grauvogel-Stamm[10], Maria E. McNamara[5,6], Hans-Dieter Sues[11] & Rainer R. Schoch[1,12]

Complex integumentary appendages such as avian feathers and mammalian hair play a principal role in tetrapod evolution, with critical functions in insulation, sensation, display and flight. Although feathers and hair originated in the stem-lineages of birds and mammals, respectively[1,2], their underlying gene regulatory network has much deeper amniote roots[3]. The early evolution of amniote integumentary appendages, however, remains poorly understood because of the absence of fossil evidence. Here we present *Mirasaura grauvogeli*, a small-sized diapsid from the Middle Triassic epoch (about 247 million years ago) with a distinctive crest formed by elongate integumentary appendages extending serially along its back, similar to those of the poorly understood Triassic reptile *Longisquama*[4–7]. Despite its superficially bird-like skull, *Mirasaura* is not closely related to avemetatarsalians but instead belongs to the exclusively Triassic reptilian clade Drepanosauromorpha[8]. Melanosomes preserved in its integumentary appendages are consistent in geometry with melanosomes of feathers but not those of reptilian skin or mammalian hair. Nevertheless, the morphology of the integumentary appendages and phylogenetic placement of *Mirasaura* indicate that they are not structurally homologous to feathers or other integumentary appendages in living amniotes. Our findings show that complex integumentary appendages are not restricted to avemetatarsalians and mammaliaforms among amniotes and evolved in a lineage basal to all extant reptiles, challenging our understanding of the evolution of the reptilian integument.

Amniotes are characterized by various types of integumentary structures, including scales, hair, horns, claws and feathers. These integumentary structures encompass a vast array of sizes and morphologies in extant and fossil amniotes that develop by means of specialized dermo–epidermal interactions. During embryogenesis, feathers, hairs and most scales follow similar trajectories of placode formation and dermal condensation regulated by shared Wnt, β-catenin, EDAR, BMP and Shh morphogen pathways[9–11]. In mammalian hair and avian feathers, the epidermal placode is subsequently invaginated into the dermis to form a follicle[12,13]. Fibrous corneous β-proteins (formerly β-keratins) that form feathers, claws and scales in reptiles probably originated in the Carboniferous[14], and most of the conserved non-exonic elements (a group of non-protein coding DNA segments) associated with corneous β-protein production are also ancestral to amniotes[3]. Thus, key elements of the genetic toolkit required to produce complex integumentary appendages are not restricted to avemetatarsalians and (stem-)mammals.

Until now, the only fossil evidence for complex integumentary appendages in reptiles outside Avemetatarsalia comes from *Longisquama insignis*, a small diapsid reptile from the Middle or Late Triassic epoch of Kyrgyzstan. This taxon was previously interpreted as an early archosaur that possessed 'protofeathers'[5,7] comprising elongate appendages projecting from the dorsal side of the animal. These appendages have since been found to differ fundamentally from pennaceous feathers in various regards (for example, refs. 4,6), including the absence of barbs. Interpretations of *Longisquama* have subsequently remained highly contentious because of preservation of the integumentary appendages as sediment casts. Furthermore, the phylogenetic position of *Longisquama* has remained unresolved, and consequently this taxon has largely been omitted from recent discussions on the evolution of the reptile integument.

Here we present an approximately 247-million-year-old Triassic diapsid with striking integumentary appendages. It is represented by

[1]Staatliches Museum für Naturkunde Stuttgart, Stuttgart, Germany. [2]Institut für Biowissenschaften, Allgemeine und Spezielle Zoologie, Universität Rostock, Rostock, Germany. [3]Museum für Naturkunde Berlin, Leibniz-Institut für Evolutions- und Biodiversitätsforschung, Berlin, Germany. [4]Department of Geosciences, University of Fribourg, Fribourg, Switzerland. [5]School of Biological, Earth and Environmental Sciences, University College Cork, Cork, Ireland. [6]Environmental Research Institute, University College Cork, Cork, Ireland. [7]School of Environment, Geography, and Geosciences, University of Portsmouth, Portsmouth, UK. [8]European Synchrotron Radiation Facility, Grenoble, France. [9]Dipartimento di Scienze Chimiche e Geologiche, Università degli Studi di Modena e Reggio Emilia, Modena, Italy. [10]Ecole et Observatoire des Sciences de la Terre, Université de Strasbourg, Strasbourg, France. [11]Department of Paleobiology, National Museum of Natural History, Washington, DC, USA. [12]Fachgebiet Paläontologie, Institut für Biologie, Universität Hohenheim, Stuttgart, Germany. ✉e-mail: stephanspiekman@gmail.com

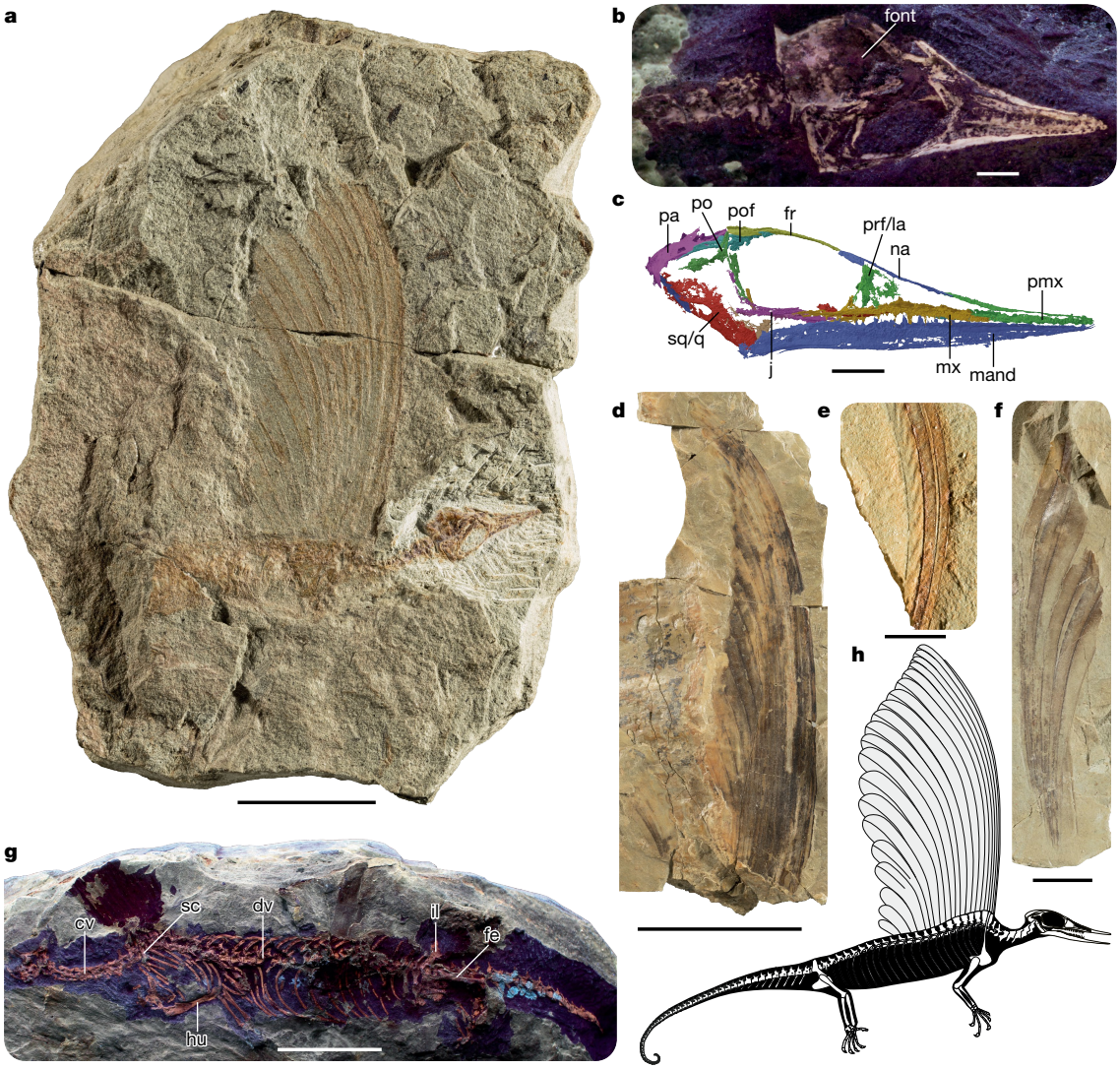

Fig. 1 | The anatomy of *M. grauvogeli*. **a**, The holotype SMNS 97278, preserving the skull, partial postcranial skeleton and crest. **b**, Skull of SMNS 97278 under ultraviolet (UV) light. **c**, Skull reconstruction of SMNS 97278 based on the synchrotron radiation microcomputed tomographic scan (mirrored). **d**, SMNS 97280, largely complete isolated crest. **e**, SMNS 97286, two overlapping integumentary appendages preserving distinct rugae. **f**, SMNS 97281, associated integumentary appendages. **g**, SMNS 97279, preserving a partial skull and impressions of a crest and a largely complete postcranial skeleton under UV light. **h**, Skeletal drawing of *Mirasaura*, based on the skull reconstruction of SMNS 97278, the postcranial anatomy of SMNS 97279 and the crests of SMNS 97278, SMNS 97281 and SMNS 97280. The morphology of the manus, part of the pes and posterior tail region is largely unknown for *Mirasaura*; the manus and pes are reconstructed on the basis of *Vallesaurus cenensis* and *Megalancosaurus preonensis*, respectively[8], whereas the grasping morphology of the tail is based on the morphology present in other known drepanosauromorphs except *Hypuronector*[8]. Scale bars, 20 mm (**a**,**g**), 2 mm (**b**,**c**), 50 mm (**d**), 5 mm (**e**), 10 mm (**f**). cv, cervical vertebra; dv, dorsal vertebra; fe, femur; font, fontanelle; fr, frontal; hu, humerus; il, ilium; j, jugal; la, lacrimal; mand, mandible; mx, maxilla; na, nasal; pa, parietal; pmx, premaxilla; po, postorbital; pof, postfrontal; prf, prefrontal; q, quadrate; sc, scapula; sq, squamosal.

two well-preserved skeletons that are associated with integumentary appendages and by 80 specimens comprising isolated integumentary appendages that preserve carbonaceous soft tissues (Fig. 1, Extended Data Figs. 1 and 2 and Supplementary Information). Investigation of the integumentary appendages shows a distally expanded bilateral morphology and preserved melanosomes that are similar in geometry to melanosomes in feathers (Fig. 2). The absence of branching in the appendages of the new taxon, however, indicates that these bilateral structures formed independently of avemetatarsalian feathers. Instead, comparisons of the skeletal and integumentary anatomy between the new species and *Longisquama* show that both are closely related taxa in Drepanosauromorpha, an exclusively Triassic clade of non-saurian diapsids. Collectively, these data challenge the hypothesis that complex integumentary appendages are unique to avemetatarsalians and derived synapsids among amniotes.

Systematic palaeontology

Diapsida Osborn, 1903
Drepanosauromorpha Renesto, Spielmann, Lucas & Spagnoli, 2010
Mirasaura grauvogeli gen. et sp. nov.

Etymology. *mirus* (Latin): wonderful or marvellous; *saura* (Latin): reptile. The species name honours Louis Grauvogel, who extensively excavated the Grès à Voltzia localities and discovered *Mirasaura*.
Holotype. SMNS 97278 (Staatliches Museum für Naturkunde Stuttgart, Germany), an articulated skull and poorly preserved postcranium, including a largely complete crest.
Referred material. SMNS 97279, a partial skull, largely complete postcranium and incomplete imprint of a crest; SMNS 97280, a large

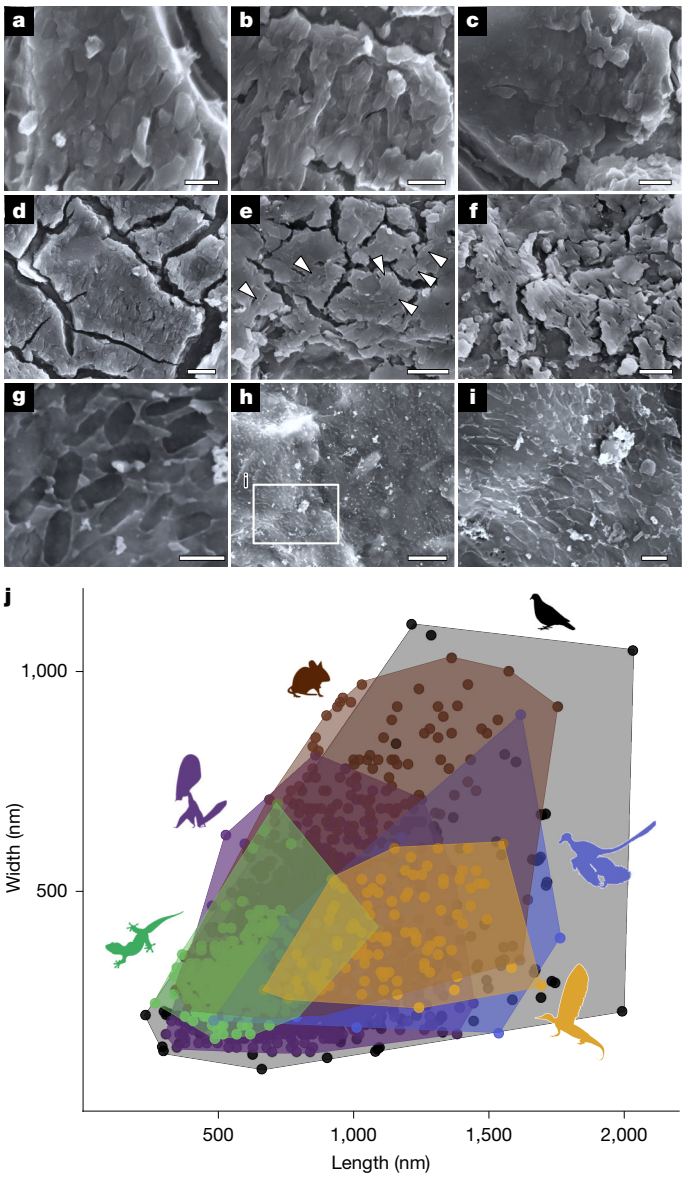

Fig. 2 | Melanosomes and melanosome geometry. a–**c**, Three-dimensionally preserved melanosomes in SMNS 97280. **d**–**f**, Three-dimensionally preserved melanosomes in SMNS 97300. **g**–**i**, Mouldic melanosomes in SMNS 97310. **j**, Morphospace of melanosomes in extant and fossil reptile skin, avian and pterosaur feathers, mammalian hairs and the integumentary appendages of *Mirasaura*. Scale bars, 1 µm (**a**,**g**,**i**), 2 µm (**b**–**f**), 5 µm (**h**). The complete melanosome dataset is presented in Supplementary Table 12 (available at https://doi.org/10.6084/m9.figshare.27083092). Data for *Mirasaura* were collected during this study, whereas the other melanosome data are derived from refs. 32,47 as collated averages, and from refs. 2,33,48,49 as raw data from individual melanosomes; *Mirasaura* (n = 100), Aves (n = 239), Pterosauria (n = 3046), Mammalia (n = 200), Reptilia (n = 353) and Theropoda (n = 60). Credits: Silhouettes were obtained from Phylopic (https://www.phylopic.org/). *Microraptor zhaoianus*, created by B. McFeeters and vectorized by T. Michael Keesey under a CC0 1.0 Universal Public Domain licence; *Patagioenas*, created by F. Sayol under a CC0 1.0 Universal Public Domain licence; *Mus musculus*, created by Mozillian under a CC0 1.0 Universal Public Domain licence; *Tupandactylus imperator*, created by E. Boucher under a Public Domain Mark 1.0 licence; and *Gehyra mutilata*, created by G. Murali under a CC0 1.0 Universal Public Domain licence.

and largely complete crest; SMNS 97281, a partial crest with excellent preservation of individual appendages; SMNS 97338, a large and largely complete impression of a crest; SMNS 97337, a partial crest; SMNS 97282–97336 and SMNS 97339–97359, 76 specimens representing remains of disarticulated integumentary appendages, occurring alone or as associated elements of up to three appendages.

Locality and horizon. Lower unit (Grès à meules) of the Grès à Voltzia Formation (early Anisian, early Middle Triassic), Vosges mountains, eastern France[15] (see Supplementary Information for geological context).

Diagnosis. *Mirasaura grauvogeli* is a drepanosauromorph distinguished by the following combination of character states (autapomorphies among non-saurian diapsids are marked with an asterisk*): elongate integumentary appendages extending dorsally from the anterior part of the trunk; long, narrow snout; dome-like skull roof; anterior portions of the jaws completely edentulous*; dorsoventrally low maxilla; frontal strongly constricted anteriorly; forward-facing orbits; transversely wide parietal; elongate, barrel-shaped trunk; seven cervical vertebrae; 24 dorsal vertebrae*; hypapophyses on cervical vertebrae; cervical ribs and gastralia absent; moderately elongate caudal haemal spines; narrow and elongate scapular blade; carpals lacking proximal elongation; ilium with tall, anterodorsally oriented blade; and large, curved pedal unguals.

Description

Skeletal anatomy

The tiny skull (total length, 17 mm; Supplementary Table 1) of the holotype SMNS 97278 is characterized by an elongate, tapering snout, large orbits and a dome-like skull roof (Fig. 1c). This configuration is typical among Drepanosauromorpha[8,16] and superficially resembles that of birds and pterosaurs. The jaws are edentulous anteriorly and bear slender, pointed teeth more posteriorly. Combined with the long, gracile snout, these features of the skull seem appropriate for probing for insects and other small invertebrates from narrow crevices. The dome-like skull roof is predominantly formed by transversely wide frontals and parietals. This resembles the condition in *Avicranium*, in which the skull roof is part of a highly encephalized skull with a large endocast relative to body size[16]. As in the drepanosauromorphs *Avicranium* and *Megalancosaurus*[16,17], the eyes face distinctly forward (Extended Data Fig. 3d). A large unossified opening (fontanelle) is present between the parietals and frontals in SMNS 97278 (Fig. 1b), indicating an early ontogenetic stage for this individual. This is consistent with its diminutive size among the *Mirasaura* material (crest height is 51 mm versus more than 153 mm in SMNS 97280). The posterior margin of the skull is distinctly inclined posterodorsally (40°) in lateral view (Fig. 1c), a feature shared with *Longisquama*, *Megalancosaurus*, *Vallesaurus* and *Avicranium*[7,17–19]. The well-preserved left maxilla and the mandible show that antorbital and mandibular fenestrae—classic archosauriform synapomorphies[20]—are unambiguously absent. The elongate nasal has a ventrolateral process near its posterior end that is separated from the main body by a distinct notch, which forms the posterodorsal corner of the external naris as in other drepanosauromorphs[17,19]. The jugal lacks a distinct posterior process, and consequently the infratemporal fenestra is open ventrally, as in other early diapsids (including drepanosauromorphs)[8,21], most lepidosaurs[22] and various Mesozoic marine reptile clades[23,24], but in contrast to the fully formed infratemporal bar of most archosauriforms[20]. The palate and braincase are poorly preserved in SMNS 97278, but short, pointed teeth are unambiguously present on the fragmentary pterygoid remains (Extended Data Fig. 3g). Palatal teeth are a common trait in early diapsids but absent in most archosaurs[20].

The vertebral column of the well-preserved postcranial skeleton of SMNS 97279 consists of seven cervical, 24 dorsal and two sacral vertebrae; the ventrally curving tail is incompletely exposed (Fig. 1g). The cervical vertebrae possess hypapophyses and lack ribs, both of which represent drepanosauromorph synapomorphies (Supplementary Information). As in most other drepanosauromorphs, the trunk is long and barrel-shaped, and all dorsal ribs are single-headed. Gastralia

are absent. The preserved tail is dorsoventrally deep, but not to the extent seen in some other drepanosauromorphs (for example, *Hypuronector*)[8,25]. Except for *Longisquama*[7] and possibly *Hypuronector*[25], *Mirasaura* shares the presence of a pronounced 'hump' in the anteriormost portion of the trunk with other drepanosauromorphs[8]. The 'hump' in *Mirasaura* is formed by the convex curvature of the vertebral column and a limited dorsal elongation of the neural spines. Its position corresponds to the anterior portion of the integumentary crest, as is evident from SMNS 97279 and SMNS 97278 (Fig. 1 and Extended Data Fig. 1a,d,e). Soft-tissue remains are present in the same region in the holotype of *Drepanosaurus unguicaudatus*, but although it has been tentatively suggested that they might belong to an integumentary crest as in *Longisquama*[8], the region is insufficiently preserved to determine this with confidence.

The scapulocoracoid of SMNS 97279 is fragmentary, but the scapular blade is clearly dorsoventrally tall and anteroposteriorly very narrow (Fig. 1g and Extended Data Fig. 1e), as in other drepanosauromorphs[8]. The forelimb lacks derived drepanosaurid features, such as an enormous crescent-shaped ulna and proximal elongation of carpal elements[26]. The humerus is considerably longer than the radius and ulna and slightly longer than the femur (Supplementary Table 2). The ulna possesses an olecranon process, which is absent in *Longisquama*[7]. The ilium is characteristically drepanosauromorph, with an iliac blade that is dorsoventrally taller than anteroposteriorly long and has an anterodorsally extending long axis[8]. The pes is only partially preserved, but the large, curved unguals and the elongation of the preungual phalanx in digits III and IV indicate an arboreal mode of life for *Mirasaura*[27].

Soft-tissue anatomy and ultrastructure

The integumentary appendages of *Mirasaura* extend dorsally along the midline of the anterior part of the trunk in SMNS 97278 and SMNS 97279 (Fig. 1a,g). The soft tissues are poorly preserved and evident as impressions with patchy orange staining. In SMNS 97278, the soft-tissue structures are vertically oriented and form a crest of 16 serial, elongated and unbranched integumentary appendages that overlap tightly. The integumentary appendages gradually decrease in height posteriorly, with the anteriormost appendage being both the proximodistally longest and anteroposteriorly narrowest; it is roughly four times the height of the posteriormost appendage (Fig. 1a). SMNS 97279 preserves only the proximal part of the crest, which is closely associated with the 'hump' of the vertebral column (Fig. 1g and Extended Data Fig. 1d,e). There is no evidence that individual integumentary appendages are directly associated with specific vertebrae: the bases of the integumentary appendages are not preserved, and there is no evidence of preserved skin or any other soft-tissue structures connecting the appendages and vertebrae. The remaining specimens of *Mirasaura* represent integumentary appendages without associated skeletal remains. Most of these isolated appendages are organically preserved; the carbon film that defines the structures varies in tone and may be absent locally. The largest isolated crest consists of 20 tightly overlapping integumentary appendages (SMNS 97280; Fig. 1d); the proximal and distal termini are not preserved. The crest has a distinctly and continuously convex anterior margin and a posterior margin that is concave in its distal portion; the posterior portion of the crest is poorly preserved and partially displaced post mortem.

The individual appendages are divided into an anteroposteriorly narrow proximal section with straight margins and a gradually expanding and posterodorsally curving distal portion. The narrow proximal section comprises at least two-thirds of the total length of the anterior appendages but becomes relatively shorter posteriorly. The proximal section is formed by three distinct bands, of which the central band is the widest (Extended Data Fig. 2a,b). The expanded distal section of each individual appendage consists of two laminae that are separated by a distinct medial structure. The laminae are asymmetrical, with the posterior lamina being slightly wider than the anterior lamina (Extended Data Figs. 2g–i and 4). The medial structure can appear as a pair of closely spaced, subparallel dark lines, where the anteriormost of the pair is darker in tone. The medial structure widens gradually towards the distal part of the appendage (Extended Data Fig. 4e). The margins of the laminae are visible as dark lines that are (sub-)parallel to the medial structure. Scanning electron microscopy (SEM) and energy dispersive X-ray spectroscopy analysis shows that dark-toned regions of the integumentary appendages are rich in C (Extended Data Fig. 5). Synchrotron rapid scanning X-ray fluorescence (SRS-XRF) imaging shows that these carbon-rich regions are associated with Fe, Ni and Cu and, to a lesser extent, Mn (Extended Data Fig. 6 and Supplementary Information). These elemental maps also aid in visualizing the medial structure and laminae. The Cu map for specimen SMNS 97280 (Extended Data Fig. 4b) shows that the distal part of the medial structure is evident as a pair of sharply defined parallel lines with striking tonal contrast on either side of each line. Furthermore, analysis of the topography of the appendage surfaces shows that the lines that define the margins of the laminae and the medial structure are regions of high topographic relief (that is, narrow, elevated ridges; Extended Data Fig. 7). The distal ends of the integumentary appendages are not clearly exposed in any specimen: the plane of splitting does not extend to the tips, which are consistently either covered by sediment or fractured and lost from the slab surface. This poor splitting reflects the lack of well-defined lamination of the sediment, which instead shows, at best, crude lamination.

The integumentary appendages are in many (but not all) cases distinctly corrugated (Extended Data Fig. 2). In the proximal portion of the integumentary appendages, a series of curved and/or horizontally oriented rugae (that is, wrinkles or folds) that are roughly equally spaced often occur in the central band. The distal portion of the integumentary appendages exhibits rugae in various orientations, ranging from horizontal to oblique, with oblique rugae oriented in either a lateroventral or a laterodorsal direction (Extended Data Fig. 2g–i). Similar structures are present in the integumentary appendages of *Longisquama*[4,6]. The rugae are variable in geometry, distribution and orientation[28], and the surface of the appendages, including the rugae, was to some extent malleable, as is clearly indicated by the irregular creases and asymmetrical patterning of the rugae in several specimens (Extended Data Fig. 2a,g). Although distinct and regular compartmentalization or branching through the rugae can thus be excluded, their nature cannot be fully resolved. They might have formed a semiregular external ridging of the appendages in life, as external sculpturing also occurs in scales of pangolins and some extant lepidosaurs[29,30]. Alternatively, the rugae could plausibly represent taphonomic artefacts resulting from contractional dehydration and/or decay established in the fibrillar keratinous tissue. The presence of rugae in both *Mirasaura* and *Longisquama*, despite their distinct preservation as mostly carbonaceous films and as external moulds, respectively, does not exclude a taphonomic origin for the rugae but rather reflects elements of common tissue structure and composition and the timing of specific post-mortem events during diagenesis. The preservation of rugae in *Longisquama* specifically can be readily explained by diagenetic cementation of the host sediment following contraction of the tissue structure, but before complete decay. Decay of the soft tissues proceeded to completeness only after extensive cementation of the sediment.

SEM imaging of the carbonaceous soft tissues shows rod-shaped to ovoid microstructures, which are preserved either as external moulds or as discrete three-dimensional microbodies that are locally abundant and mutually aligned (Fig. 2a–i) (1,143 ± 207 nm long and 412 ± 97 nm wide; $n = 100$). The geometry of these microstructures is consistent with that of melanosomes in extant and fossil vertebrates[31–35]; the geometry is not consistent with that of modern bacteria[28,36]. These microstructures are therefore interpreted as fossil melanosomes. This interpretation is supported by the carbonaceous composition of the soft-tissue film. The length and width of the melanosomes in *Mirasaura*

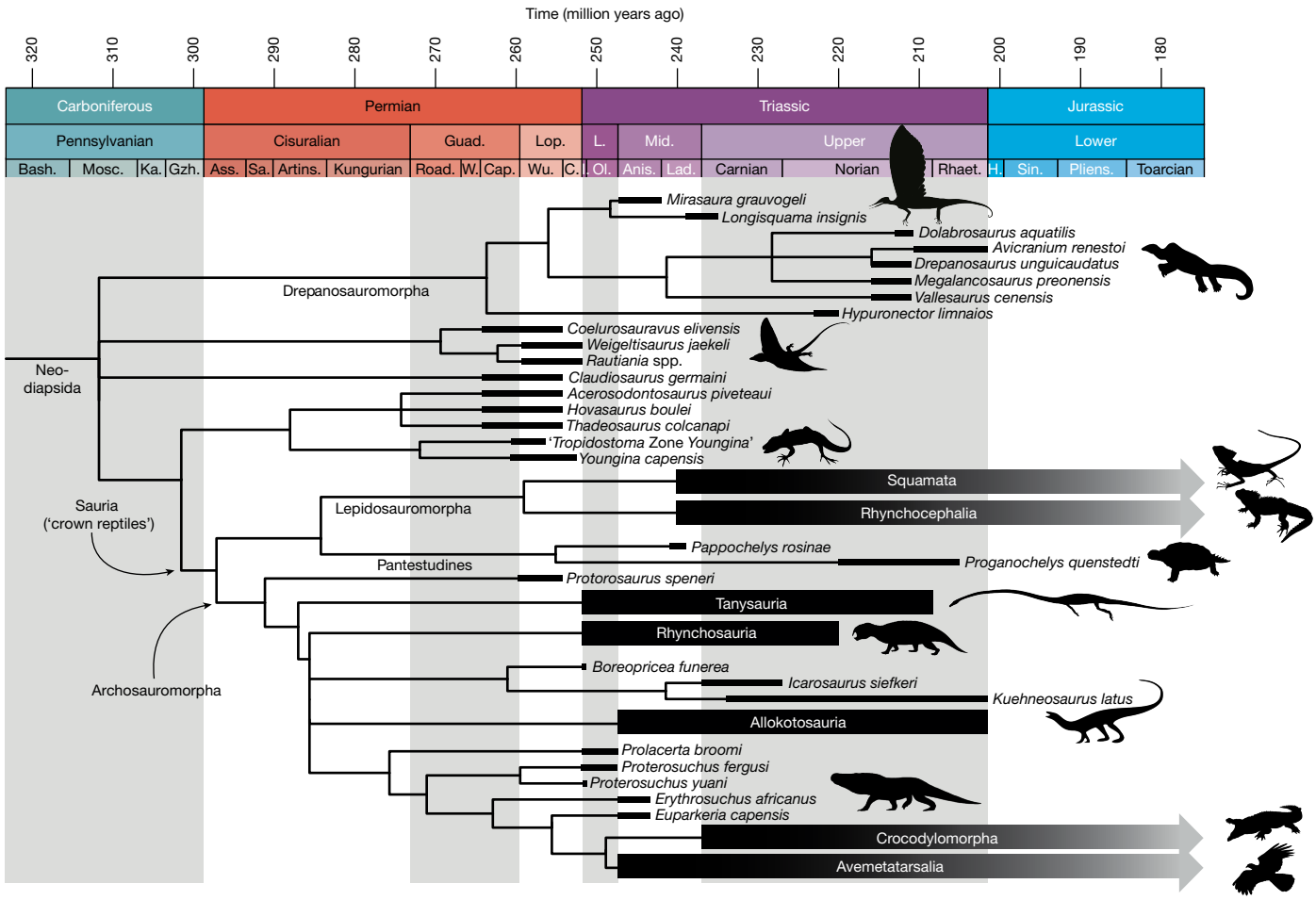

Fig. 3 | Time-calibrated majority rule consensus tree of neodiapsid interrelationships. For the complete tree and support values, see Extended Data Fig. 10a. The lengths of the black bars indicate the known temporal stratigraphic range of each terminal taxon. Credits: Silhouettes were obtained from Phylopic (www.phylopic.org). *Drepanosaurus unguicaudatus*, created by X. A. Jenkins and G. Ugueto under a CC0 1.0 Universal Public Domain licence; *Weigeltisaurus jaekeli*, created by S. Reid under an Attribution 3.0 Unported licence; *Youngina capensis*, created by B. McFeeters and vectorized by T. Michael Keesey under a CC0 1.0 Universal Public Domain licence; *Laemanctus serratus*, created by J. C. Arenas-Monroy under a CC0 1.0 Universal Public Domain licence; *Sphenodon punctatus*, created by S. Traver under a CC0 1.0 Universal Public Domain licence; *Hyperodapedon*, created by S. Traver under a CC0 1.0 Universal Public Domain licence; *Malerisaurus robinsonae*, created by N. Tamura under an Attribution 4.0 International licence; *Garjainia madiba*, created by M. Witton under an Attribution 3.0 Unported licence; *Crocodylus porosus*, created by S. Traver under a CC0 1.0 Universal Public Domain licence; and *Ibycter americanus*, created by S. McCann under a CC0 1.0 Universal Public Domain licence. The silhouette of *Tanystropheus* is adapted with permission from ref. 50, Cell Press. Anis., Anisian; Artins., Artinskian; Ass., Asselian; Bash., Bashkirian; C., Changhsingian; Cap., Capitanian; Guad., Guadalupian; Gzh., Gzhelian; H., Hettangian; I., Induan; Ka., Kasimovian; L., Late; Lad., Ladinian; Lop., Lopingian; Mid., Middle; Mosc., Moscovian; Ol., Olenekian; Pliens., Pliensbachian; Rhaet., Rhaetian; Road., Roadian; Sa., Sakmarian; Sin., Sinemurian; W., Wordian; Wu., Wuchiapingian.

differ significantly from those of melanosomes in the skin of extant reptiles and in the feathers of extant birds[28] (Extended Data Fig. 8 and Supplementary Data File 13 (available at https://doi.org/10.6084/m9.figshare.27083092)). Importantly, however, the aspect ratio of the melanosomes in *Mirasaura* differs significantly from that of melanosomes from reptile skin and mammal hair, but not feathers. Aspect ratio is the most important discriminator between melanosomes in reptile skin and mammal hair (where melanosomes have a narrow range of aspect ratio values: that is, less diverse shapes) and feathers (where melanosomes have a wide range of aspect ratio values: that is, more diverse shapes)[32]. This finding—that the melanosomes of *Mirasaura* are similarly diverse in shape to those in feathers—is supported by our analysis of melanosome geometry (Fig. 2j and Extended Data Fig. 8). The morphospace of the *Mirasaura* melanosomes overlaps fully with that of extant and fossil feathers and partly with the morphospace of melanosomes from mammal hair, and only minor overlap is observed with melanosomes from reptile skin. Collectively, these analyses demonstrate that melanosomes in the integumentary appendages of *Mirasaura* cannot be distinguished morphologically from melanosomes in feathers but differ significantly from those in skin or hair.

Phylogenetic relationships

We incorporated *Mirasaura* into the most detailed available character–taxon matrix for drepanosauromorphs, closely related diapsid taxa and early members of Lepidosauromorpha and Archosauromorpha in both relevant taxon and character sampling[37]. We additionally included *Longisquama* and the stem-turtles *Pappochelys* and *Proganochelys*; the latter two were added so that early representatives of all three principal extant reptile clades are represented in the matrix. The dataset was analysed with both Bayesian and maximum parsimony algorithms[28] (Methods). *Mirasaura* is recovered in Drepanosauromorpha with strong support values (Fig. 3, Extended Data Figs. 9 and 10 and Supplementary Information). *Mirasaura* possesses the following drepanosauromorph synapomorphies on the basis of the results of the maximum parsimony analyses: postaxial cervical vertebrae with saddle-shaped intervertebral

articular surface (heterocoely), cervical ribs absent as distinct ossifications, haemal spines substantially longer than caudal neural spines, long axis of iliac blade anterodorsally oriented, and posterior process of ilium weakly developed and not extending well posterior to acetabulum. Despite the previous controversy surrounding the systematic position of *Longisquama*, our re-examination of this taxon shows several features that also support its placement in Drepanosauromorpha, including the presence of a tapering snout and dome-like skull roof, a distinctly slanted posterior skull margin and the absence of cervical ribs (Supplementary Information). Drepanosauromorphs were previously exclusively known from Late Triassic strata, with the oldest occurrence dating from the late Carnian[8]. The earliest Anisian age of *Mirasaura* therefore pushes the origin of Drepanosauromorpha back by some 20 million years, nearly doubling the known temporal range of the clade (Fig. 3).

Drepanosauromorpha is consistently recovered among stem-diapsids and outside Sauria (that is, the least-inclusive clade comprising all extant reptiles) in our analyses (Fig. 3 and Extended Data Figs. 9 and 10). Drepanosauromorphs have alternatively been placed in Archosauromorpha[8,18,38], the stem-lineage of living crocodylians and birds. To test this alternative hypothesis, we implemented a tree constraint that forced the drepanosauromorph taxa in Archosauromorpha in the equal weights maximum parsimony analysis, which required 19 additional steps to resolve the tree for our dataset. We additionally re-analysed the most recent matrix that recovered Drepanosauromorpha in Archosauromorpha[18,28]. Following our inclusion of *Mirasaura*, *Longisquama*, *Pappochelys* and *Proganochelys* and a re-evaluation of the other included drepanosauromorph taxa, we did not recover this previous result but instead found Drepanosauromorpha as the sister group to Sauria (Supplementary Information). Although our results consistently point towards a non-saurian position of Drepanosauromorpha, the exact phylogenetic placement of this clade remains poorly supported because of limited available drepanosauromorph material and the highly derived anatomy of all drepanosauromorphs known at present, which includes many skeletal specializations for an arboreal and/or digging mode of life. Nevertheless, the absence of several key archosauriform synapomorphies, such as antorbital and mandibular fenestrae and a closed infratemporal bar, unambiguously places Drepanosauromorpha outside Archosauriformes. *Mirasaura* is, therefore, only distantly related to archosaurs and, on the basis of the oldest known archosauriform, *Archosaurus*, diverged from the lineage leading to avemetatarsalians by the middle or late Permian, but probably considerably earlier[39].

Homology with *Longisquama* and function

In both *Mirasaura* and *Longisquama*, the integumentary appendages form a tall crest along the dorsal midline of the anterior part of the trunk[4,7] (Fig. 1h). The individual appendages of both species possess a low aspect ratio with a narrow proximal portion that is horizontally subdivided in three bands and that expands distally into a distinct bilateral structure with a medial structure (described as a 'middle axis' for *Longisquama*[4]) (Extended Data Figs. 2 and 4). Both species also show distinct rugae on their integumentary appendages. In these shared features, the appendages of *Mirasaura* and *Longisquama* are distinct from other reptilian integumentary derivatives, including known feather morphotypes (see 'Implications for integumentary evolution' below). Considering also the close phylogenetic relationships between the two taxa (Fig. 3, Extended Data Figs. 9 and 10 and Supplementary Information), we therefore conclude that their integumentary appendages are homologous (that is, they have a shared origin from a common ancestor).

Although the exact function (that is, the biological role) of the integumentary crest of *Mirasaura* and *Longisquama* remains uncertain in the absence of extant analogues, a function in gliding flight or body insulation can be excluded, because the elongate integumentary appendages of both species are restricted to a single, unpaired row along the dorsal midline or the anterior part of the trunk[4] (Fig. 1a,g). It is also unlikely that the crest served for mimicry either through camouflage or by deterring predators by resembling a potentially harmful organism (Batesian mimicry)[40], because the crest of *Mirasaura* does not resemble the shape of any other known taxon from the Grès à Voltzia[15,41]. Instead, the large size of the crest and its vertical orientation indicate that a role in visual communication (in particular, intraspecific signalling and/or predator deterrence) is most likely. *Mirasaura* probably had good visual acuity based on its large, anteriorly facing orbits and inferred arboreal habits. The vertebral 'hump' possibly served to accentuate the crest. It has been suggested that the crest of *Longisquama* could be folded back across the body[4]. However, in all preserved examples of *Mirasaura*, the crest is oriented vertically, and it seems unlikely that musculature attaching to the narrow base of the appendages could achieve the roughly 90° rotation required to drape the appendages posteriorly across the body.

Implications for integumentary evolution

The integumentary appendages of *Mirasaura* and *Longisquama* are distinct from known skin crests, scales, horns and hair of other amniotes in their highly consistent and organized morphology, comprising a proximal portion with a wide central band and a distal, expanded portion that is characterized by two laminae separated by a distinct medial structure (see Supplementary Information for more details). Furthermore, these appendages are remarkably long relative to body size and exhibit a low aspect ratio with a very narrow proximal base and a gradual distal expansion, which is unlike known scale morphotypes. Finally, the geometry of preserved melanosomes demonstrates a significant distinction between the integumentary appendages of *Mirasaura* and both hair and scaly reptile skin[28] (Fig. 2j). The strong tissue specificity of melanosomes in extant vertebrates is well known[32,33]. We can therefore exclude a close affinity for the integumentary appendages of *Mirasaura* and *Longisquama* to both scaly skin and hair.

The integumentary appendages resemble pennaceous feathers in their expanded distal bilateral morphology and the presence of a medial structure, which superficially look like the vane and rachis, respectively, of pennaceous feathers. Remarkably, the melanosome geometry of the *Mirasaura* appendages is also consistent with that of feathers[28] (Fig. 2j and Extended Data Fig. 8). The integumentary appendages of both *Mirasaura* and *Longisquama*, however, differ from pennaceous feathers in the absence of branching; instead, each lamina of the appendage forms a continuous layer, as indicated by the dark carbonaceous film preserved on most specimens (Fig. 1c,e). In bilaterally symmetrical feathers, the rachis forms by helical displacement and proximal fusion of barbs on the anterior side of the developing feather, and the feather tube unfolds into the paired vanes on either side of the rachis[42,43]. The rachis is thus a direct derivative of the branched barbs. Because barbs are not apparent in the integumentary appendages of *Mirasaura* and *Longisquama*, the medial structure cannot be considered homologous to the rachis. Together with the results of our phylogenetic analyses, which indicate a Palaeozoic non-saurian diapsid as the last common ancestor for *Mirasaura* and avemetatarsalians (Fig. 3), this indicates that the bilateral integumentary appendages in drepanosauromorphs and avemetatarsalians evolved independently from each other.

The evolution of feathers and hair is considered to have played a crucial role in the evolutionary success of both archosaurs and mammaliaforms in what has been named the 'Triassic arms race'[44], facilitating the acquisition of endothermy and enlarged brains by providing body insulation[44–46]. We confirm the presence of structurally complex integumentary appendages among a third group of amniotes, the drepanosauromorphs. Unlike mammaliaforms and archosaurs, drepanosauromorphs did not survive into the Jurassic, and their

integumentary appendages probably served for visual display rather than insulation. This expands the known evolutionary drivers for the origin of complex integumentary appendages among amniotes. Furthermore, the presence of structurally distinct integumentary appendages in the non-saurian drepanosauromorphs highlights the importance of the Triassic as a time of evolutionary innovation. These findings confirm that highly elongate and structurally complex integumentary appendages were present among non-avemetatarsalian diapsids and possibly even preceded the origin of modern reptiles, reshaping our understanding of reptile evolution.

Online content

Any methods, additional references, Nature Portfolio reporting summaries, source data, extended data, supplementary information, acknowledgements, peer review information; details of author contributions and competing interests; and statements of data and code availability are available at https://doi.org/10.1038/s41586-025-09167-9.

1. Ji, Q., Luo, Z.-X., Yuan, C.-X. & Tabrum, A. R. A swimming mammaliaform from the Middle Jurassic and ecomorphological diversification of early mammals. *Science* **311**, 1123–1127 (2006).
2. Yang, Z. et al. Pterosaur integumentary structures with complex feather-like branching. *Nat. Ecol. Evol.* **3**, 24–30 (2019).
3. Lowe, C. B., Clarke, J. A., Baker, A. J., Haussler, D. & Edwards, S. V. Feather development genes and associated regulatory innovation predate the origin of Dinosauria. *Mol. Biol. Evol.* **32**, 23–28 (2015).
4. Buchwitz, M. & Voigt, S. The dorsal appendages of the Triassic reptile *Longisquama insignis*: reconsideration of a controversial integument type. *Palaontol. Z.* **86**, 313–331 (2012).
5. Jones, T. D. et al. Nonavian feathers in a Late Triassic archosaur. *Science* **288**, 2202–2205 (2000).
6. Reisz, R. R. & Sues, H.-D. The 'feathers' of *Longisquama*. *Nature* **408**, 428–428 (2000).
7. Sharov, A. G. [Unusual reptile from the Lower Triassic of Fergana]. *Paleontol. Zh.* **1**, 127–131 (1970).
8. Renesto, S., Spielmann, J. A., Lucas, S. G. & Spagnoli, G. T. The taxonomy and paleobiology of the Late Triassic (Carnian-Norian: Adamanian-Apachean) drepanosaurs (Diapsida: Archosauromorpha: Drepanosauromorpha). *Bull. New Mexico Mus. Nat. Hist. Sci.* **46**, 1–81 2010).
9. Dhouailly, D. et al. Getting to the root of scales, feather and hair: as deep as odontodes? *Exp. Dermatol.* **28**, 503–508 (2019).
10. Di-Poï, N. & Milinkovitch, M. C. The anatomical placode in reptile scale morphogenesis indicates shared ancestry among skin appendages in amniotes. *Sci. Adv.* **2**, e1600708 (2016).
11. Musser, J. M., Wagner, G. P. & Prum, R. O. Nuclear β-catenin localization supports homology of feathers, avian scutate scales, and alligator scales in early development. *Evol. Dev.* **17**, 185–194 (2015).
12. Widelitz, R. B., Veltmaat, J. M., Mayer, J. A., Foley, J. & Chuong, C.-M. Mammary glands and feathers: comparing two skin appendages which help define novel classes during vertebrate evolution. *Semin. Cell Dev. Biol.* **18**, 255–266 (2007).
13. Millar, S. E. Molecular mechanisms regulating hair follicle development. *J. Invest. Dermatol.* **118**, 216–225 (2002).
14. Dalla Valle, L. et al. β-keratins of the crocodilian epidermis: composition, structure, and phylogenetic relationships. *J. Exp. Zool. B Mol. Dev. Evol.* **312**, 42–57 (2009).
15. Gall, J.-C. Faunes et paysages du Grès à Voltzia du Nord des Vosges. Essai paléoécologique sur le Buntsandstein supérieur. *Mémoires du Service de la Carte géologique d'Alsace et de Lorraine* **34**, 1–318 (1971).
16. Pritchard, A. C. & Nesbitt, S. J. A bird-like skull in a Triassic diapsid reptile increases heterogeneity of the morphological and phylogenetic radiation of Diapsida. *R. Soc. Open Sci.* **4**, 170499 (2017).
17. Renesto, S. & Dalla Vecchia, F. M. The skull and lower jaw of the holotype of *Megalancosaurus preonensis* (Diapsida, Drepanosauridae) from the Upper Triassic of Northern Italy. *Riv. Ital. Paleontol. Stratigr.* **111**, 247–257 (2005).
18. Buffa, V., Frey, E., Steyer, J.-S. & Laurin, M. 'Birds' of two feathers: *Avicranium renestoi* and the paraphyly of bird-headed reptiles (Diapsida: 'Avicephala'). *Zool. J. Linn. Soc.* **202**, zlae050 (2024).
19. Renesto, S. & Binelli, G. *Vallesaurus cenensis* Wild, 1991, a drepanosaurid (Reptilia, Diapsida) from the Late Triassic of northern Italy. *Riv. Ital. Paleontol. Stratigr.* **112**, 77–94 (2006).
20. Ezcurra, M. D. The phylogenetic relationships of basal archosauromorphs, with an emphasis on the systematics of proterosuchian archosauriforms. *PeerJ* **4**, e1778 (2016).
21. Spiekman, S. N. F., Fraser, N. C. & Scheyer, T. M. A new phylogenetic hypothesis of Tanystropheidae (Diapsida, Archosauromorpha) and other "protorosaurs", and its implications for the early evolution of stem archosaurs. *PeerJ* **9**, e11143 (2021).
22. Evans, S. E. in *Biology of the Reptilia* Vol. 20 (eds Gans, C. et al.) Ch. 1 (Society for the Study of Amphibians and Reptiles, 2008).
23. Moon, B. C. & Kirton, A. M. Ichthyosaurs of the British Middle and Upper Jurassic Part 1. *Ophthalmosaurus*. *Monogr. Palaeontogr. Soc.* **170**, 1–84 (2016).
24. Rieppel, O. *Sauropterygia I: Placodontia, Pachypleurosauria, Nothosauroidea, Pistosauroidea*. *Handbuch der Paläoherpetologie* Vol. 12A (Verlag Dr. Friedrich Pfeil, 2000).
25. Colbert, E. H. & Olsen, P. E. A new and unusual aquatic reptile from the Lockatong Formation of New Jersey (Late Triassic, Newark Supergroup). *Am. Mus. Novit.* **2001**, 1–24 (2001).
26. Pritchard, A. C., Turner, A. H., Irmis, R. B., Nesbitt, S. J. & Smith, N. D. Extreme modification of the tetrapod forelimb in a Triassic diapsid reptile. *Curr. Biol.* **26**, 1–8 (2016).
27. Hopson, J. A. in *New Perspectives on the Origin and Early Evolution of Birds: Proc. of the International Symposium in Honor of John H. Ostrom* (eds Gauthier, J. & Gall, I. F.) Ch. 12 (Peabody Museum of Natural History, 2001).
28. Spiekman, S.N.F. et al. Supplementary Files to 'Triassic diapsid shows early diversification of skin appendages in reptiles'. *Figshare* https://doi.org/10.6084/m9.figshare.27083092 (2025).
29. Chang, C. et al. Reptile scale paradigm: Evo-Devo, pattern formation and regeneration. *Int. J. Dev. Biol.* **53**, 813 (2009).
30. Wang, B., Yang, W., Sherman, V. R. & Meyers, M. A. Pangolin armor: overlapping, structure, and mechanical properties of the keratinous scales. *Acta Biomater.* **41**, 60–74 (2016).
31. Edwards, N. P. et al. Elemental characterisation of melanin in feathers via synchrotron X-ray imaging and absorption spectroscopy. *Sci. Rep.* **6**, 34002 (2016).
32. Li, Q. et al. Melanosome evolution indicates a key physiological shift within feathered dinosaurs. *Nature* **507**, 350–353 (2014).
33. Rossi, V., McNamara, M. E., Webb, S. M., Ito, S. & Wakamatsu, K. Tissue-specific geometry and chemistry of modern and fossilized melanosomes reveal internal anatomy of extinct vertebrates. *Proc. Natl Acad. Sci. USA* **116**, 17880–17889 (2019).
34. Wogelius, R. A. et al. Trace metals as biomarkers for eumelanin pigment in the fossil record. *Science* **333**, 1622–1626 (2011).
35. Rossi, V., Webb, S. M. & McNamara, M. E. Hierarchical biota-level and taxonomic controls on the chemistry of fossil melanosomes revealed using synchrotron X-ray fluorescence. *Sci. Rep.* **10**, 8970 (2020).
36. Roy, A. et al. in *Pennaraptoran Theropod Dinosaurs Past Progress and New Frontiers* (eds Pittman, M. & Xu, X.) Ch. 9 (American Museum of Natural History, 2020).
37. Pritchard, A. C., Sues, H.-D., Scott, D. & Reisz, R. R. Osteology, relationships and functional morphology of *Weigeltisaurus jaekeli* (Diapsida, Weigeltisauridae) based on a complete skeleton from the Upper Permian Kupferschiefer of Germany. *PeerJ* **9**, e11413 (2021).
38. Simões, T. R. et al. The origin of squamates revealed by a Middle Triassic lizard from the Italian Alps. *Nature* **557**, 706–709 (2018).
39. Ezcurra, M. D., Scheyer, T. M. & Butler, R. J. The origin and early evolution of Sauria: reassessing the Permian saurian fossil record and the timing of the crocodile-lizard divergence. *PLoS ONE* **9**, e89165 (2014).
40. Caro, T. Antipredator deception in terrestrial vertebrates. *Curr. Zool.* **60**, 16–25 (2014).
41. Grauvogel-Stamm, L. La flore du Grés à Voltzia (Buntsandstein supérieur) des Vosges du Nord (France): morphologie, anatomie, interprétations phylogénique et paléogéographique. *Sci. Géologiques, Bull. et. Mémoires* **50**, 1–225 (1978).
42. Lucas, A. M. & Stettenheim, P. R. *Avian Anatomy. Integument, Part I and II* (US Government Printing Office, 1972).
43. Prum, R. O. Development and evolutionary origin of feathers. *J. Exp. Zool. B Mol. Dev. Evol.* **285**, 291–306 (1999).
44. Benton, M. J. The origin of endothermy in synapsids and archosaurs and arms races in the Triassic. *Gondwana Res.* **100**, 261–289 (2021).
45. Benton, M. J., Dhouailly, D., Jiang, B. & McNamara, M. The early origin of feathers. *Trends Ecol. Evol.* **34**, 856–869 (2019).
46. Olsen, P. et al. Arctic ice and the ecological rise of the dinosaurs. *Sci. Adv.* **8**, eabo6342 (2022).
47. Babarović, F. et al. Characterization of melanosomes involved in the production of non-iridescent structural feather colours and their detection in the fossil record. *J. R. Soc. Interface* **16**, 20180921 (2019).
48. Cincotta, A. et al. Pterosaur melanosomes support signalling functions for early feathers. *Nature* **604**, 684–688 (2022).
49. Hu, D. et al. A bony-crested Jurassic dinosaur with evidence of iridescent plumage highlights complexity in early paravian evolution. *Nat. Commun.* **9**, 217 (2018).
50. Spiekman, S. N. F. et al. Aquatic habits and niche partitioning in the extraordinarily long-necked Triassic reptile. *Tanystropheus*. *Curr. Biol.* **30**, 3889–3895 (2020).

Methods

Phylogenetic analyses

The phylogenetic relationships of *Mirasaura* were investigated using the data matrix of ref. 37. This represents the most detailed matrix available for sampling both relevant taxa and characters for drepanosauromorphs, closely related diapsid taxa and early members of the extant clades Lepidosauromorpha and Archosauromorpha. We added *Mirasaura* and *Longisquama* to the matrix, plus the stem-turtles *Pappochelys*[51,52] and *Proganochelys*[53]. We excluded *Colobops*, as it was previously misinterpreted in this matrix[54,55]. We added a single character to the matrix (character 340, elongate and complex integumentary appendages dorsal to anterior dorsal vertebrae: (0) absent in fully articulated specimens preserving the trunk, (1) present). Soft tissues rarely fossilize, making it difficult to confidently ascertain the absence of soft-tissue structures in extinct taxa in vivo; to account for this uncertainty, all analyses were run both including and excluding this character. Following ref. 56, characters 1, 4, 7, 19, 20, 25, 28, 30, 40, 58, 60, 88, 97, 100, 113, 123, 152, 166, 183, 191, 196, 233, 276, 305 and 316 were treated as additive and *Petrolacosaurus* was set as the outgroup.

Maximum parsimony analyses were performed in TNT v.1.6 (ref. 57) under both equal weights and extended implied weighting[58]. Determining an appropriate weighting value (k) in implied weighting parsimony is dependent on the number of terminal taxa included. On the basis of a comparison between several widely used morphological character matrices, the optimal k-value for different numbers of terminal taxa was recently established for palaeontological phylogenetic datasets[59], and the matrix used here, consisting of 64 terminal taxa, corresponds to a preferred value of $k = 3–11$. The value for k was set at the lower end of this range ($k = 3$) to determine the influence of extended implied weighting relative to equal weighting parsimony, because a lower k-value corresponds to a larger degree of downweighting for homoplastic characters. Following ref. 60, nodes with an absolute score difference equivalent to a step in a character with homoplasy were collapsed, and relative fit was set at 0.25 for the extended implied weights analyses. For both the equal and extended implied weights analyses, tree searches were conducted using a New Technology Search with Sectorial Search, Ratchet, Drift and Tree fusing enabled. A driven search was executed until the same minimum tree length was hit 100 times. The recovered most parsimonious trees were subsequently subjected to a final round of tree bisection and reconnection branch swapping. Bremer and Bootstrap (GC) support values were calculated, the latter through a Traditional search with 1,000 iterations. Homoplasy indices were calculated with the STATSb. run script[61].

Bayesian inference analyses were executed in MrBayes v.3.2.7 (ref. 62) using the MkV model under a gamma distribution. Both uncalibrated and time-calibrated analyses were performed, the latter using relaxed-clock and fossilized birth–death models under standard parameters. In the calibrated analyses, tip calibrations were based on first and last known occurrences of each taxon (Supplementary Information). For node calibrations, we followed the recommendation of ref. 39 for Sauria (archosauromorph–lepidosauromorph split: 269.3–254.7 million years ago (Ma), and calibrations for Archosauria and Lepidosauria were set between the minimum occurrence date of their respective oldest member (Lepidosauria: *Megachirella*, 243.3 Ma (refs. 38,63); Archosauria: *Ctenosauriscus*, 247.2 Ma (refs. 64)) and the minimum age of Sauria. Root age (305.2–318 Ma) was calibrated on the basis of the minimum occurrence date of *Petrolacosaurus* and the maximum age of the earliest crown amniotes[65,66]. For all analyses, we ran metropolis-coupling Markov chain Monte Carlo sampling with two runs of four chains each and a heating coefficient of 0.05 and three swap attempts per generation. Analyses ran until average standard deviation of split frequencies decreased below 0.01, and convergence was confirmed by a potential scale reduction factor of about 1.0 and Effective Sample Sizes of greater than 200 for all parameters as recovered in Tracer v.1.7.2 (ref. 67).

Synchrotron microcomputed tomography acquisition and image processing

The skull of SMNS 97278 was imaged with propagation phase contrast synchrotron radiation microcomputed tomography at the European Synchrotron and Radiation Facility (Grenoble, France) on BM18 (ref. 68). The skull block was imaged at an isotropic voxel size of 4.04 µm (2.02 µm configured with binning of factor 2). The beamline was configured with a filtered white beam setup to an energy of 125 keV with attenuator blocks of 5-mm sapphire, silicon dioxide bars of 30 mm and 0.21-mm molybdenum with a 250-µm-thick luAg scintillator. The sample-to-detector distance was 1.5 m (ref. 69), with acquisition done with a PCO edge 4.2 sCMOS, recording 6,000 projections and a total exposure time of 15 ms, with five accumulated images of 3 ms each[70]. The skull was scanned with an offset of 800 pixels to increase final volume field of view. The final tomographic volume was reconstructed using PyHST2[71] and using the single-distance Paganin phase retrieval approach[72]. The resulting data were segmented in Mimics Research v.25.0 (https://www.materialise.com/en/medical/mimics-innovation-suite/mimics). The rendered objects were imported as PLY files into Blender v.3.2 (https://blender.org), where colours and texture were applied, individual objects were moved and rotated to create the in vivo reconstruction (following ref. 50; see Supplementary Information for further justification) and images and animations were rendered.

UV-induced fluorescence and photography

Several specimens were exposed to UV radiation to test for fluorescence of the skeletal and integumentary tissues, with only the skeletons of SMNS 97278 and SMNS 97279 being found successfully reactive for photographic documentation (Fig. 1 and Extended Data Fig. 1). Specimens were exposed to combined UV-A (peak emission at 368 nm), UV-B (peak emission at 318 nm) and UV-C (peak emission at 254 nm) wavelengths produced with a 95-W discharge lamp from Way-TooCool LLC. Pictures were taken with a Canon 700D camera with either a 24- or a 100-mm lens coupled with an orange filter to minimize collateral blue halo from the UV lamp.

SEM

Initial investigation of the soft tissues was conducted with an environmental Zeiss EVO LS15 present at the SMNS on specimens SMNS 97280, 97300, 97292, 97306, 97322, 97324, 97325, 97329 and 97341–97345. Small samples were mounted on aluminium stubs and double-sided carbon tape and sputter-coated with 6-µm gold–palladium using a Leica EM ACE 200. Sampled regions were visualized under high vacuum and secondary electron detector using a working distance of 5–10 mm, accelerating voltage of 10 kV and a probe current of 100–150 pA.

Further SEM analysis was performed using a JEOL JSM-IT100 at the University College Cork. Small samples (about 1 mm^2) were dissected using sterile tools and placed on aluminium stubs. Samples from specimens SMNS 97310 and SMNS 97280 were first examined uncoated and then gold coated. Uncoated samples were analysed at low vacuum at an accelerating voltage of 10 kV, 40 probe current and 8–10 mm working distance; coated samples were analysed at 15–20 kV, 40–60 probe current and 6–10 mm working distance. Samples from specimen SMNS 97300 were examined with an environmental FEI Quanta 200 SEM and a FEI Quanta 650 field emission gun SEM using a working distance of 8.6–13 mm, accelerating voltage of 10–30 kV and a probe current of 1.5–3.0.

Melanosome geometry

Length and width of 50 melanosomes were measured from SEM images in ImageJ, and the aspect ratios were calculated in Excel. This dataset was compared with available datasets on melanosome and

bacteria geometry from extant and fossil taxa[2,31,32,35,47,48]. Differences in melanosome geometries (that is, length, width and their aspect ratio) from different tissues were assessed statistically using analysis of variance–type statistical tests, specifically Kruskal–Wallis and Welch analysis of variance. Normality and homoscedasticity were checked using standard residual plots in R.

SRS-XRF

SRS-XRF data were collected at the Stanford Synchrotron Radiation Lightsource using beam line 7-2. The incident X-ray energy was set to 11 keV using a Si (111) double-crystal monochromator with the storage ring containing 500 mA in top-off mode at 3.0 GeV. A focused beam of 25 µm × 25 µm was provided by using a tungsten aperture. The incident X-ray intensity was measured with a nitrogen-filled ion chamber. Fossil-bearing slabs were mounted at 45° to the incident X-ray beam and were spatially rastered at 20 ms per pixel dwell time with a pixel size of 75 µm × 75 µm. The entire fluorescence spectrum was collected at each data point, and the intensity of fluorescence lines for selected elements (P, S, Cl, K, Ca, Ti, Mn, Fe, Ni, Cu and Zn) was monitored using a Vortex silicon drift detector. The concentrations of each element in µg per cm^2 were calibrated using NIST traceable thin film elemental standards. Data processing was performed using MicroAnalysis Toolkit software v.3.0.9.

Reporting summary

Further information on research design is available in the Nature Portfolio Reporting Summary linked to this article.

Data availability

Files related to the phylogenetic analyses and the analyses of melanosome geometry are available as Supplementary Information and are available at Figshare (https://doi.org/10.6084/m9.figshare.27083092)[28]. The digital models and SRµCT data of the skull of SMNS 97278 are freely available at https://doi.esrf.fr/10.15151/ESRF-DC-2206265966. The Life Science Identifier for *Mirasaura grauvogeli* is urn:lsid:zoobank.org:act:CAFF3904-B686-4DF8-81E9-4ECCEDD1606A.

Code availability

The character-taxon matrices used for the morphological phylogenetic analyses, including the code used to conduct the Bayesian analyses in MrBayes, are available at Figshare (https://doi.org/10.6084/m9.figshare.27083092)[28].

51. Schoch, R. R. & Sues, H.-D. A Middle Triassic stem-turtle and the evolution of the turtle body plan. *Nature* **523**, 584–587 (2015).
52. Schoch, R. R. & Sues, H.-D. Osteology of the Middle Triassic stem-turtle *Pappochelys rosinae* and the early evolution of the turtle skeleton. *J. Syst. Paleontol.* **16**, 927–965 (2018).
53. Gaffney, E. S. The comparative osteology of the Triassic turtle *Proganochelys*. *Bull. Am. Mus. Nat. Hist.* **194**, 1–263 (1990).
54. Pritchard, A. C., Gauthier, J. A., Hanson, M., Bever, G. S. & Bhullar, B.-A. S. A tiny Triassic saurian from Connecticut and the early evolution of the diapsid feeding apparatus. *Nat. Commun.* **9**, 1213 (2018).
55. Scheyer, T. M. et al. *Colobops*, a juvenile rhynchocephalian reptile (Lepidosauromorpha), not a diminutive archosauromorph with an unusually strong bite. *R. Soc. Open Sci.* **7**, 1–14 (2020).
56. Pritchard, A. C. & Sues, H.-D. Postcranial remains of *Teraterpeton hrynewichorum* (Reptilia: Archosauromorpha) and the mosaic evolution of the saurian postcranial skeleton. *J. Syst. Paleontol.* **17**, 1745–1765 (2019).
57. Goloboff, P. A. & Morales, M. E. TNT version 1.6, with a graphical interface for MacOS and Linux, including new routines in parallel. *Cladistics* **39**, 144–153 (2023).
58. Goloboff, P. A. Extended implied weighting. *Cladistics* **30**, 260–272 (2014).
59. Ezcurra, M. D. Exploring the effects of weighting against homoplasy in genealogies of palaeontological phylogenetic matrices. *Cladistics* **40**, 242–281 (2024).
60. Goloboff, P. A., Torres, A. & Arias, J. S. Weighted parsimony outperforms other methods of phylogenetic inference under models appropriate for morphology. *Cladistics* **34**, 407–437 (2018).
61. Spiekman, S. N. F., Ezcurra, M. D., Butler, R. J., Fraser, N. C. & Maidment, S. C. R. *Pendraig milnerae*, a new small-sized coelophysoid theropod from the Late Triassic of Wales. *R. Soc. Open Sci.* **8**, 210915 (2021).
62. Ronquist, F. et al. MrBayes 3.2: efficient Bayesian phylogenetic inference and model choice across a large model space. *Syst. Biol.* **61**, 539–542 (2012).
63. Ogg, J. G., Chen, Z.-Q., Orchard, M. J. & Jiang, H. S. in *Geologic Time Scale 2020* Vol. 2 (eds Gradstein, F. M. et al.) Ch. 25 (Elsevier, 2020).
64. Butler, R. J. et al. The sail-backed reptile *Ctenosauriscus* from the latest Early Triassic of Germany and the timing and biogeography of the early archosaur radiation. *PLoS ONE* **6**, e25693 (2011).
65. Aretz, M. et al. in *Geologic Time Scale 2020* Vol. 2 (eds Gradstein, F. M. et al.) Ch. 23 (Elsevier, 2020).
66. Benton, M. J. et al. Constraints on the timescale of animal evolutionary history. *Palaeontol. Electronica* **18**, 1–106 (2015).
67. Rambaut, A., Drummond, A. J., Xie, D., Baele, G. & Suchard, M. A. Posterior summarization in Bayesian phylogenetics using Tracer 1.7. *Syst. Biol.* **67**, 901–904 (2018).
68. Spiekman, S. N. F. Earliest evidence of 'feather-like' integumentary structures in a Middle Triassic stem-diapsid. [Dataset]. *European Synchrotron Radiation Facility* https://doi.org/10.15151/ESRF-ES-899271212 (2025).
69. Weitkamp, T., Haas, D., Wegrzynek, D. & Rack, A. ANKAphase: software for single-distance phase retrieval from inline X-ray phase-contrast radiographs. *J. Synchrotron Radiat.* **18**, 617–629 (2011).
70. Cau, A. et al. Synchrotron scanning reveals amphibious ecomorphology in a new clade of bird-like dinosaurs. *Nature* **552**, 395–399 (2017).
71. Mirone, A., Brun, E., Gouillart, E., Tafforeau, P. & Kieffer, J. The PyHST2 hybrid distributed code for high speed tomographic reconstruction with iterative reconstruction and a priori knowledge capabilities. *Nucl. Instrum. Methods Phys. Res. B* **324**, 41–48 (2014).
72. Paganin, D., Mayo, S. C., Gureyev, T. E., Miller, P. R. & Wilkins, S. W. Simultaneous phase and amplitude extraction from a single defocused image of a homogeneous object. *J. Microsc.* **206**, 33–40 (2002).

Acknowledgements We acknowledge the Gesellschaft zur Förderung des Naturkundemuseums Stuttgart (Förderverein SMNS) for facilitating the acquisition of the 'Grauvogel collection'. We thank A. C. Pritchard for sharing surface models of *Avicranium* and additional preliminary data on drepanosauromorph cranial anatomy and D. Foffa and S.W. Evers for advice on Bayesian phylogenetics. S.N.F.S. also thanks E. Amson, E. Mujal and E. E. Maxwell for helpful discussions. The TNT software program is freely available through the Willi Hennig Society. This study was supported by the Deutsche Forschungsgemeinschaft (grant no. SCHO 791/7–1 to R.R.S.) and a European Research Council Consolidator Grant (grant no. H2020-ERC-COG-101003293-PALAEOCHEM to M.E.M.). The Lauer Foundation for Paleontology, Science and Education (PSE) provided the UV equipment (three-wavelength UV lamp) and photographic filters (to G.S.).

Author contributions S.N.F.S., R.R.S., H.-D.S., D.S., O.G.B.E., L.G.-S., C.F., V.R. and M.E.M. designed the project. S.N.F.S. described the skeletal anatomy; S.N.F.S. and C.F. interpreted and described the integumentary appendages. S.N.F.S. and K.N.D. processed and sampled synchrotron µCT data. S.N.F.S. performed the phylogenetic analyses. V.R., C.G.M. and S.N.F.S. sampled the specimens and performed the SEM analyses. V.R. conducted statistical analysis on melanosome geometry. M.E.M., V.R. and T.S.S. conducted the SRS-XRF analyses. V.R. conducted data processing and interpretation of SRS-XRF data. G.S. conducted UV photography. C.G.M. created the elevation map. H.-D.S., R.R.S. and L.G.-S. provided the geological interpretation. S.N.F.S., C.F., V.R., M.E.M. and T.S. wrote the bulk of the manuscript, S.N.F.S. and V.R. prepared the figures. All the authors discussed the analyses and reviewed the manuscript.

Competing interests The authors declare no competing interests.

Additional information

Supplementary information The online version contains supplementary material available at https://doi.org/10.1038/s41586-025-09167-9.

Correspondence and requests for materials should be addressed to Stephan N. F. Spiekman.

Peer review information *Nature* thanks Michael Benton, Nicholas Fraser, Silvio Renesto and the other, anonymous, reviewer(s) for their contribution to the peer review of this work.

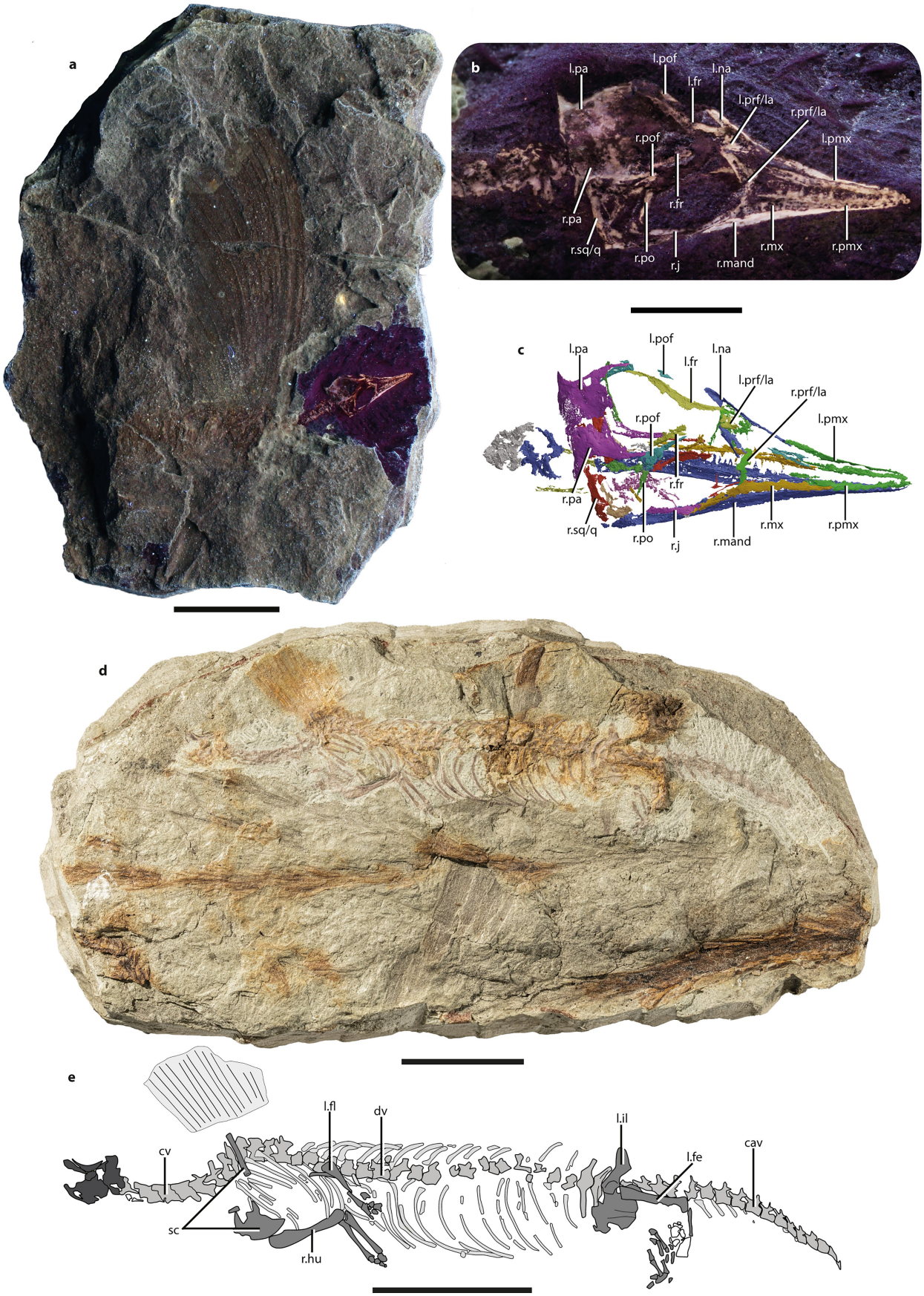

Extended Data Fig. 1 | See next page for caption.

Extended Data Fig. 1 | Selected material of *Mirasaura grauvogeli*. **a**, Holotype specimen SMNS 97278 under UV light. **b**, Skull of SMNS 97278 under UV light. **c**, Skull rendering of SMNS 97278 based on the synchrotron radiation microcomputed tomographic scan. **d**, SMNS 97279. **e**, Interpretative drawing of the anatomy of SMNS 97279. Anatomical abbreviations: cav, caudal vertebra; cv, cervical vertebra; dv, dorsal vertebra; fe, femur; fl, forelimb; fr, frontal; hu, humerus; il, ilium; j, jugal; l., left; la, lacrimal; mand, mandibular ramus; mx, maxilla; na, nasal; pa, parietal; pmx, premaxilla; po, postorbital; pof, postfrontal; prf, prefrontal; q, quadrate; r., right; sc, scapula; sq, squamosal. Scale bars, 20 mm (**a, d-e**), 5 mm (**b-c**).

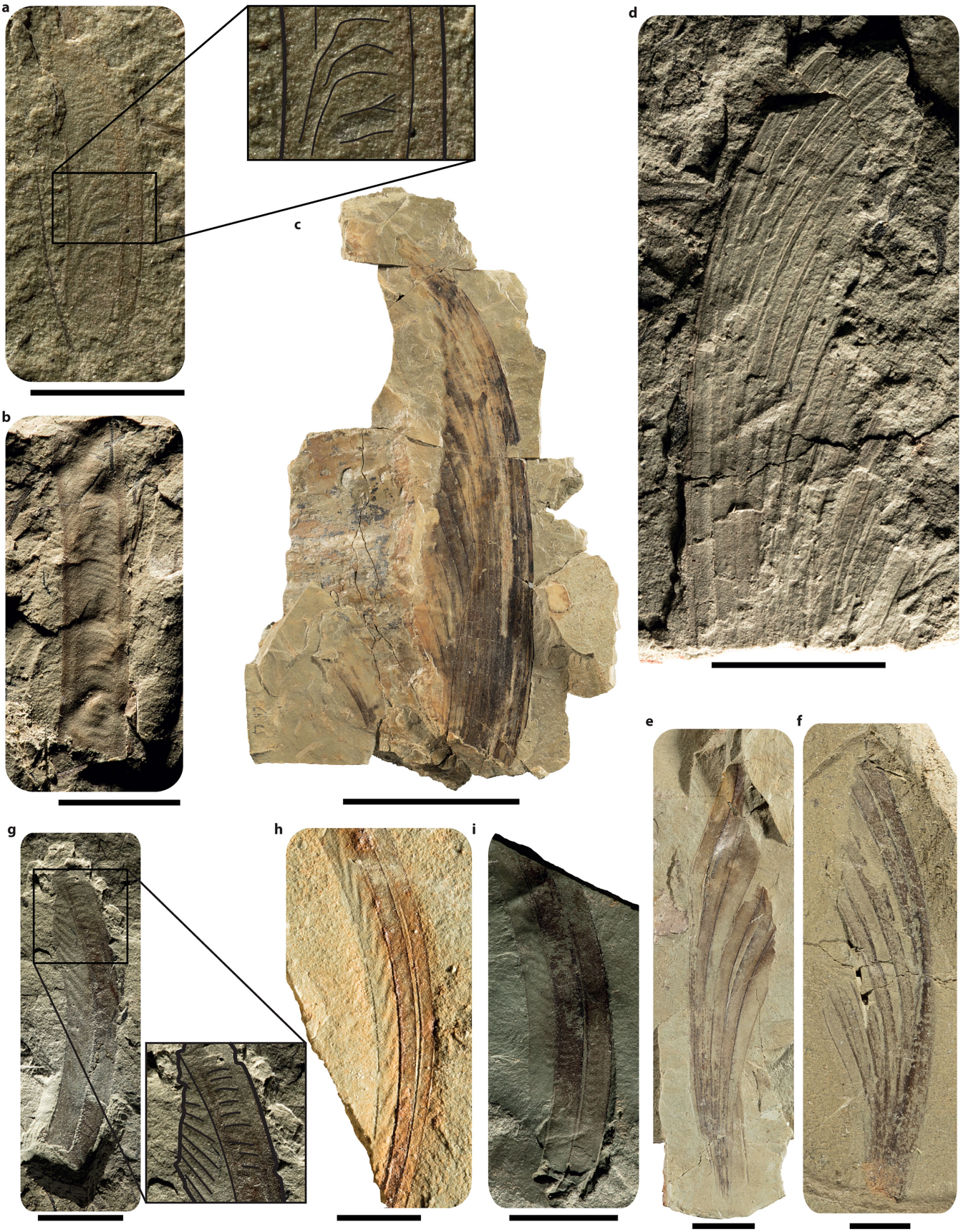

Extended Data Fig. 2 | See next page for caption.

Extended Data Fig. 2 | Selected specimens of *Mirasaura grauvogeli* preserving integumentary appendages. a, SMNS 97304, an isolated appendage preserving the proximal portion. **b**, SMNS 97333, an isolated appendage preserving the proximal portion. **c**, SMNS 97280, a largely complete crest. **d**, SMNS 97338, an impression of a largely complete crest lacking the proximal region. **e**, SMNS 97281, a bundle of four integumentary appendages. **f**, SMNS 97337, a bundle of around seven integumentary appendages. **g**, SMNS 97300, an isolated appendage preserving the distal portion. **h**, SMNS 97286, two overlapping integumentary appendages preserving the distal portion. **i**, SMNS 97342, two overlapping integumentary appendages preserving the distal portion. Black boxes indicate regions of variation in ruga morphology, highlighting the malleability of the rugae in the appendages. Scale bars, 5 mm (**a, f, h**), 10 mm (**b, e, g, i**), 50 mm (**c**), 20 mm (**d**).

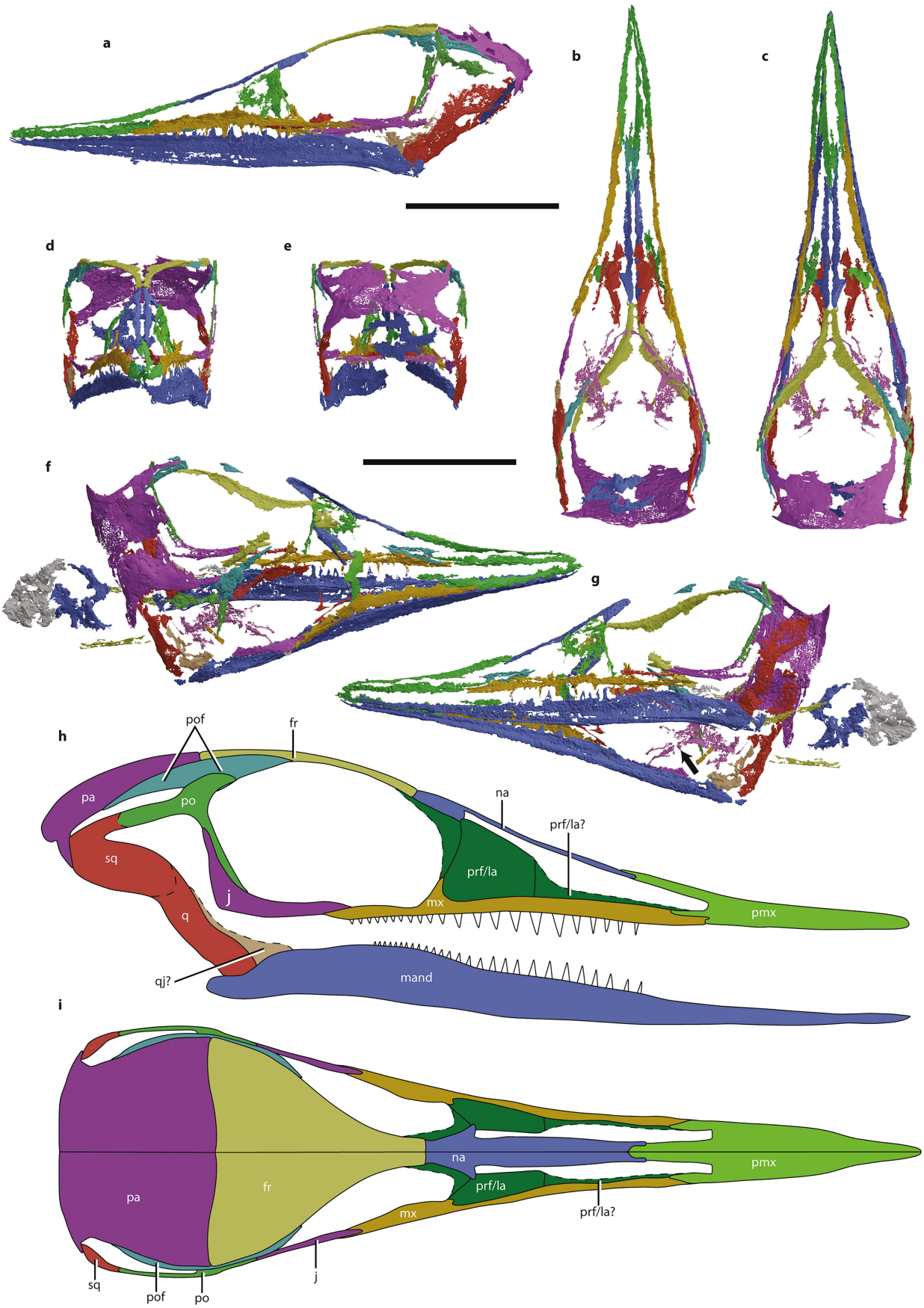

Extended Data Fig. 3 | See next page for caption.

Extended Data Fig. 3 | The skull of *Mirasaura grauvogeli*. **a**, In vivo skull restoration of SMNS 97278 based on the synchrotron radiation microcomputed tomographic scan in left lateral view. **b**, Same as **a** in ventral view. **c**, Same as **a** in dorsal view. **d**, Same as **a** in anterior view. **e**, Same as **a** in posterior view. **f**, In situ skull reconstruction of SMNS 97278 based on the synchrotron radiation microcomputed tomographic scan as exposed in external view. **g**, Opposite view of **f**; the black arrow points towards the teeth preserved on the pterygoid. **h**, Skull reconstruction of *Mirasaura grauvogeli* in right lateral view. **i**, same as **h** in dorsal view. Anatomical abbreviations: fr, frontal; j, jugal; la, lacrimal; mand, mandible; mx, maxilla; na, nasal; pa, parietal; pmx, premaxilla; po, postorbital; pof, postfrontal; prf, prefrontal; q, quadrate; qj, quadratojugal; sq, squamosal. Scale bars are 5 mm.

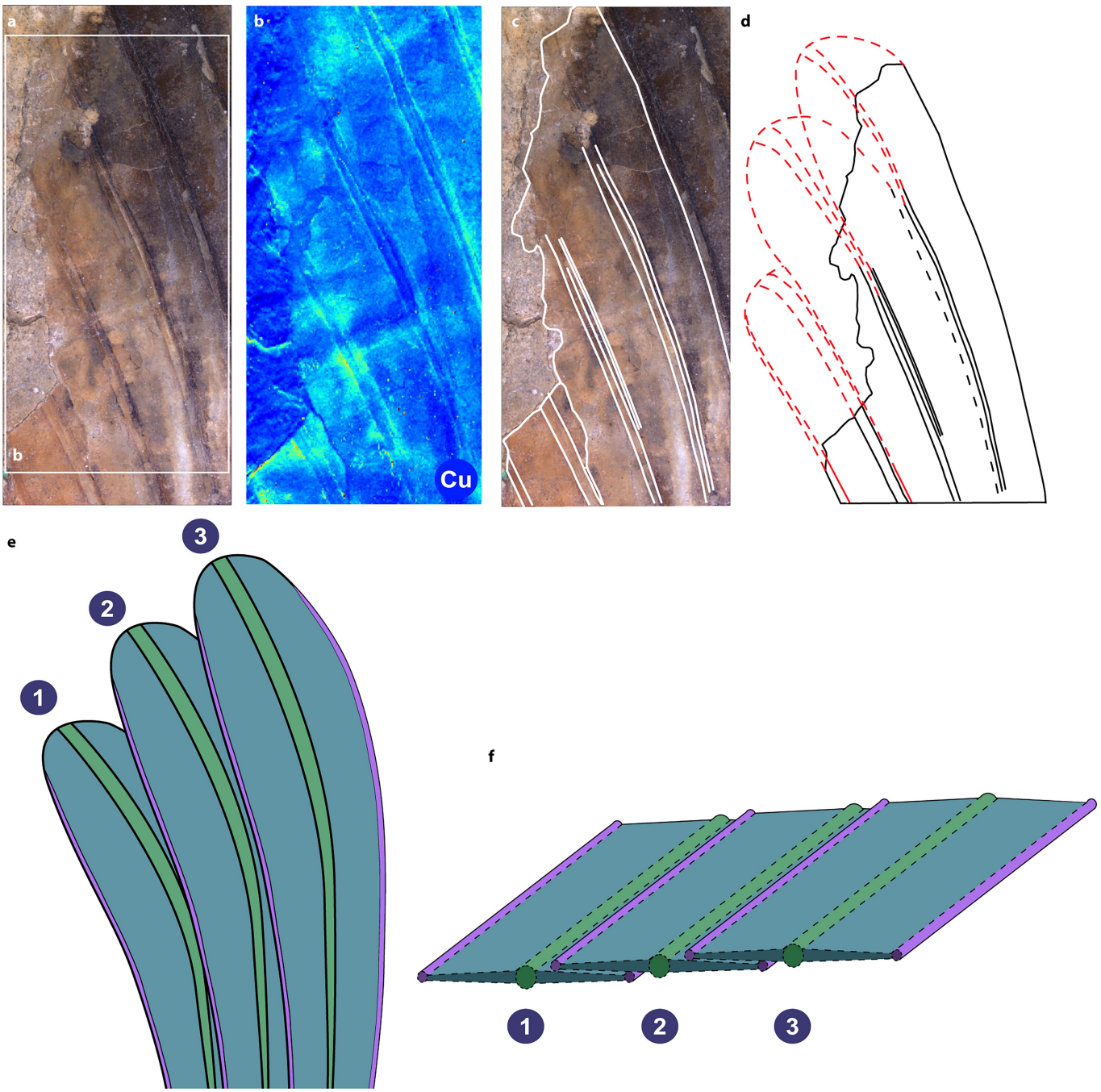

Extended Data Fig. 4 | Geometry of overlapping integumentary appendages in *Mirasaura*. **a**, Detail of selected area of the crest of SMNS 97280. White rectangle denotes the region analysed. **b**, Elemental map showing the spatial distribution of Cu. **c-d**, Interpretative drawings based on the Cu map of the structural features associated with the integumentary appendages. Red lines indicate interpretative reconstructions of regions where the soft tissues are not preserved. **e**, Simplified schematic reconstruction of three overlapping laminae in lateral view. Colours denotes margins (purple), laminae (sky blue) and medial structure (green). **f**, Interpretative schematic reconstruction of the three appendages in cross section, showing their overlapping geometry.

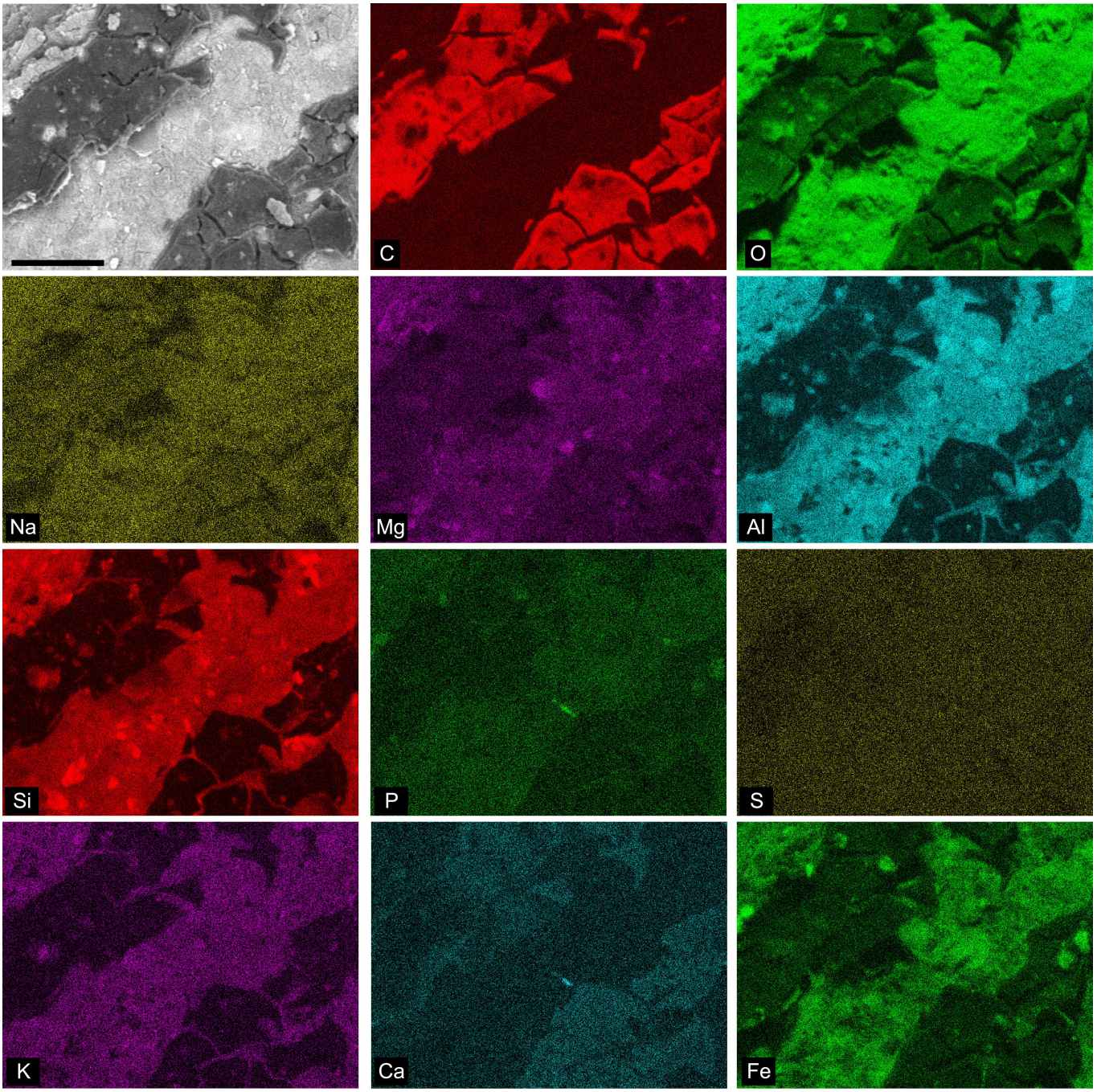

Extended Data Fig. 5 | SEM-EDS element maps. Sample of carbon-rich film dissected from specimen SMNS 97280 (see Supplementary Information for more details). Scale bar is 30 µm.

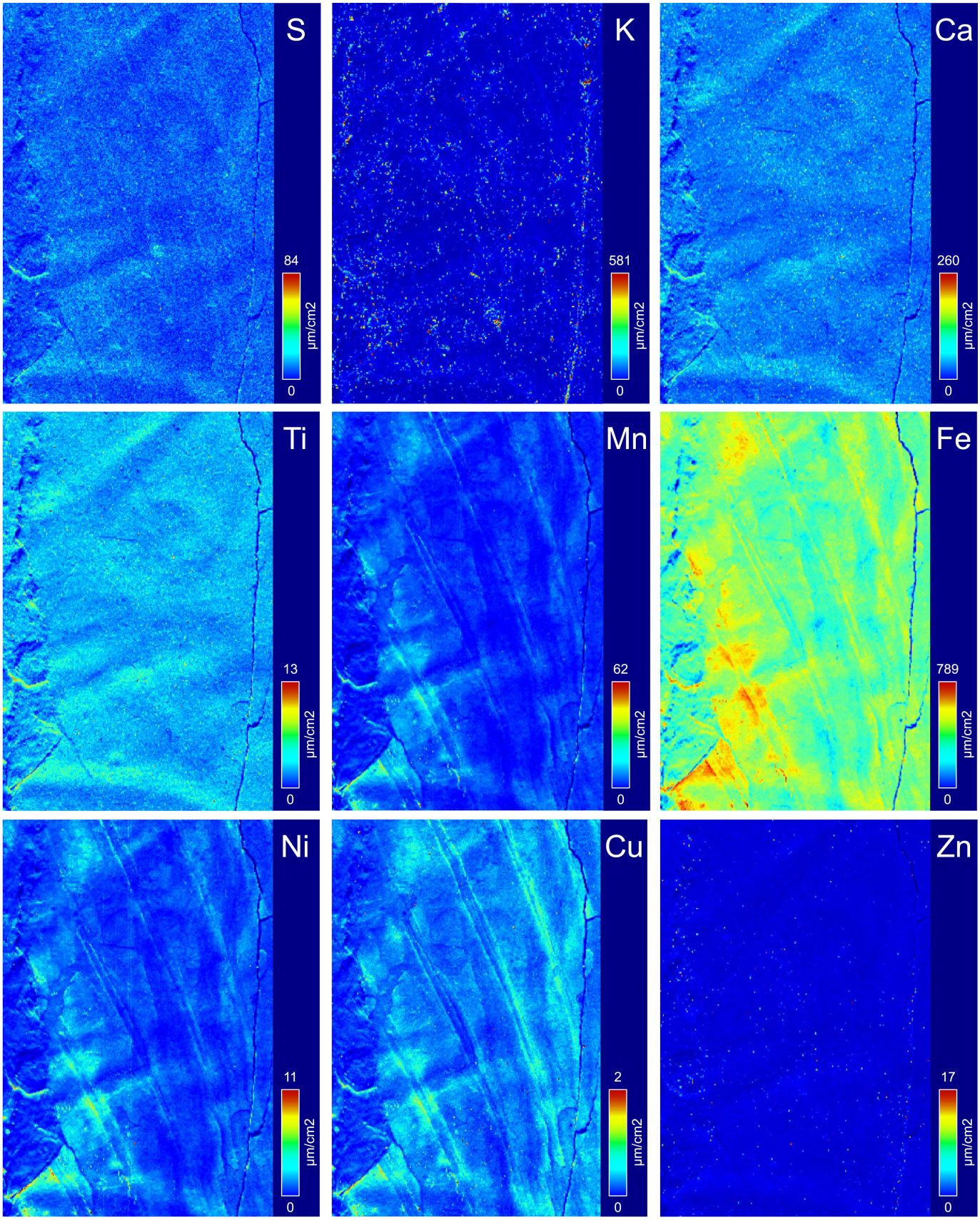

Extended Data Fig. 6 | SRS-XRF element maps. Posterior proximal preserved region of SMNS 97280 (see Supplementary Information for more details).

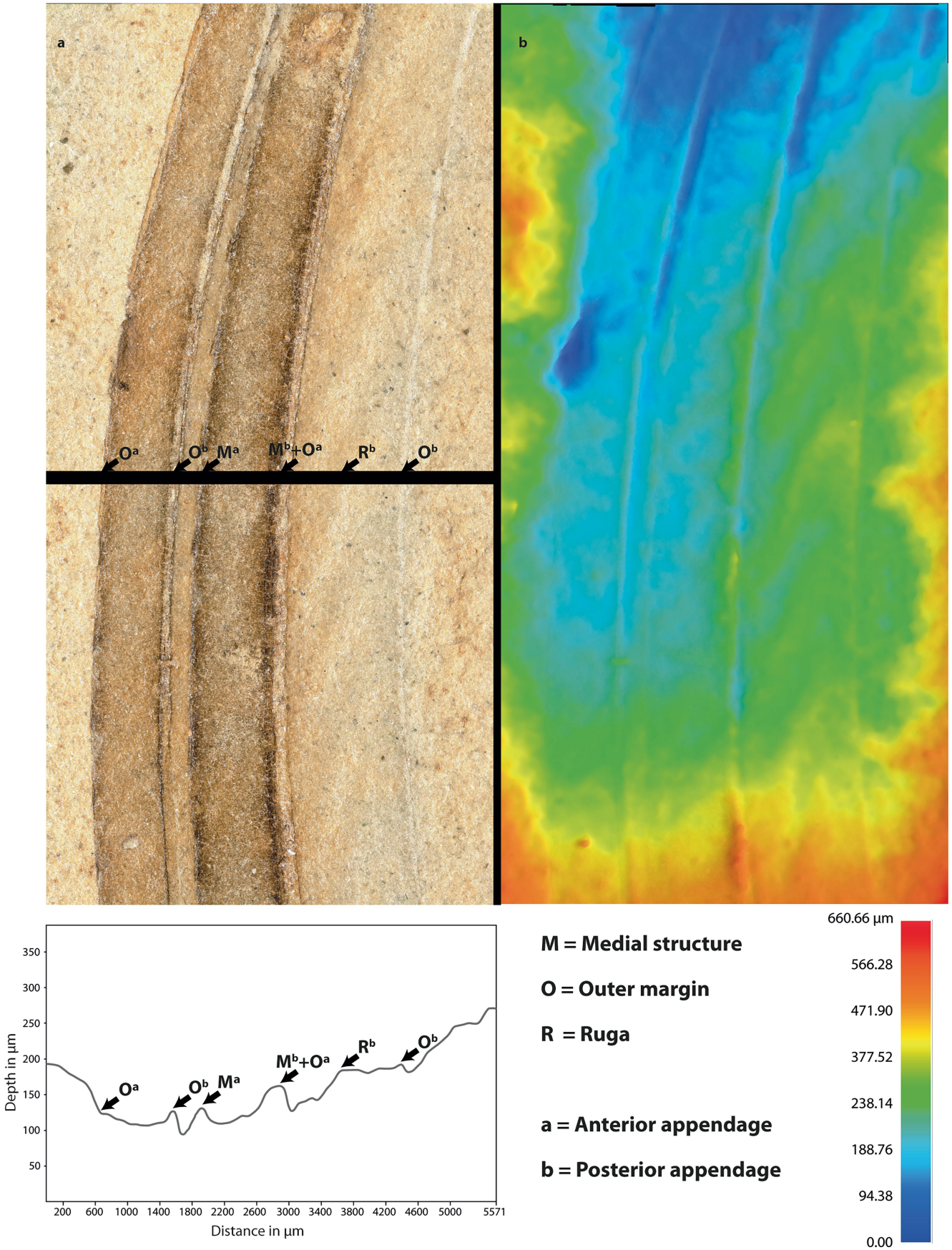

Extended Data Fig. 7 | Elevation map of two overlapping integumentary appendages in SMNS 97286. a, Photograph with elevation profile chart (below) measured at the level of the horizontal line. Arrows indicate peaks in the chart that correspond to morphological features in the two respective appendages. See horizontal axis for figure scale; **b**, False colour depth map.

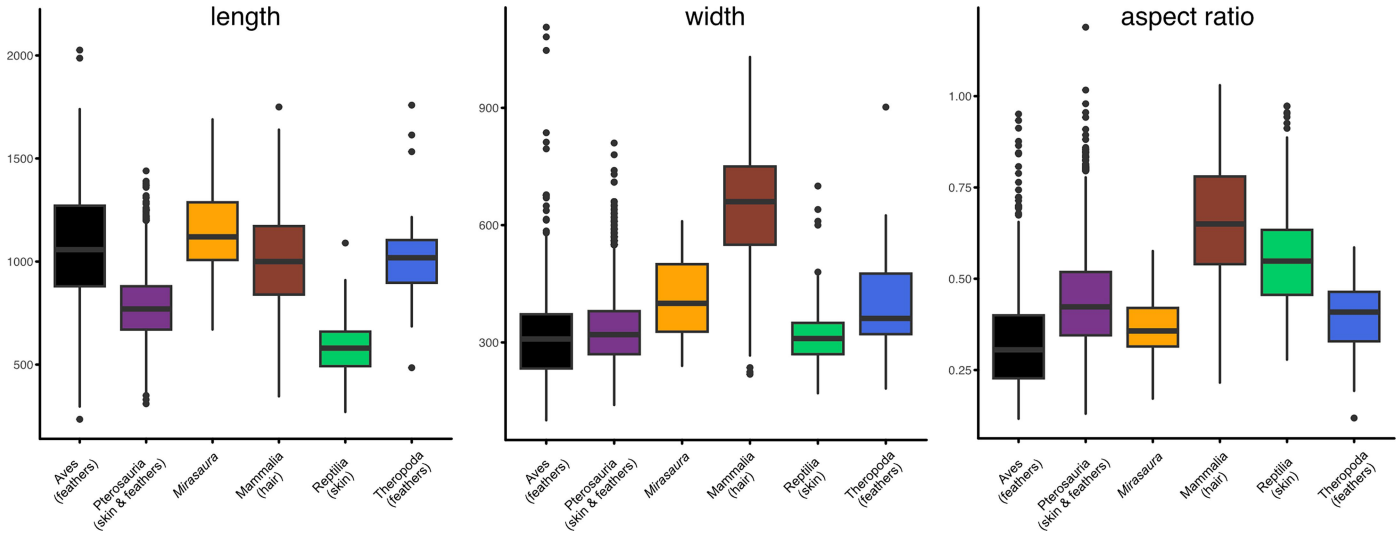

Extended Data Fig. 8 | Box plots of length, width and aspect ratio of melanosomes in feathers, hair, skin and *Mirasaura* soft tissues. The thick middle black line in each box plot denotes the median. Length and width are provided in nanometres (nm). The full dataset is provided in Supplementary Table 12 (see also the caption of Fig. 2).

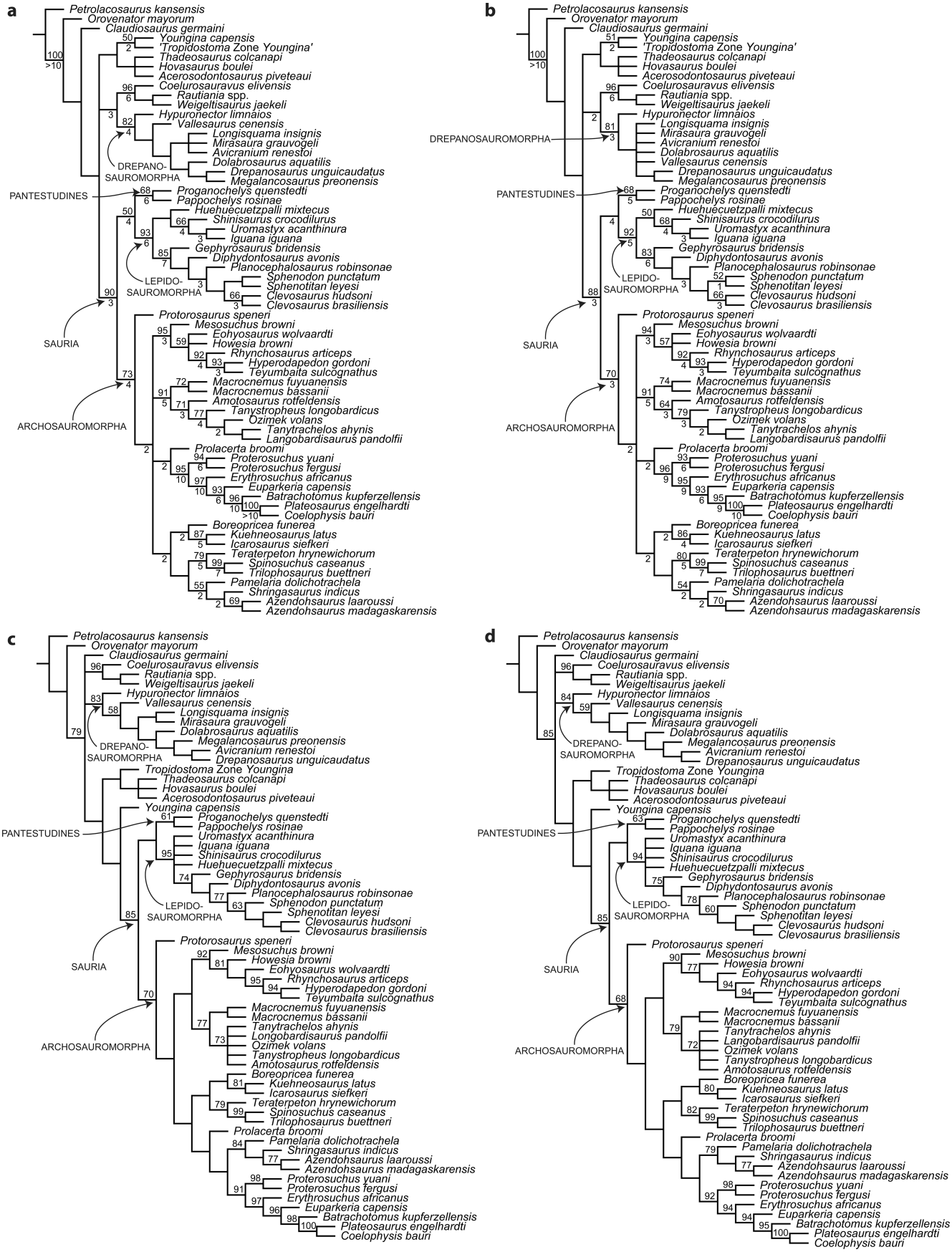

Extended Data Fig. 9 | See next page for caption.

Extended Data Fig. 9 | Maximum parsimony analyses results. a, Strict consensus tree of the equal weights analysis including character 340 (out of six most parsimonious trees of 1299 steps. CI [Consistency index] = 0.291; RI [Retention index] = 0.637). **b**, Strict consensus tree of the equal weights analysis excluding character 340 (out of 36 most parsimonious trees of 1298 steps. CI = 0.290; RI = 0.637). **c**, Strict consensus tree of the extended implied weights analysis (k = 3) including character 340 (out of 35 best fitting trees. Fit = 118.22376-118.82376). **d**, Strict consensus tree of the extended implied weights analysis (k = 3) excluding character 340 (out of 35 best fitting trees. Fit = 118.21364-118.81364.). Bootstrap GC frequencies >50% are listed above each node for the equal and extended implied weights analyses; Bremer supports >1 are listed below each node for the equal weights analysis.

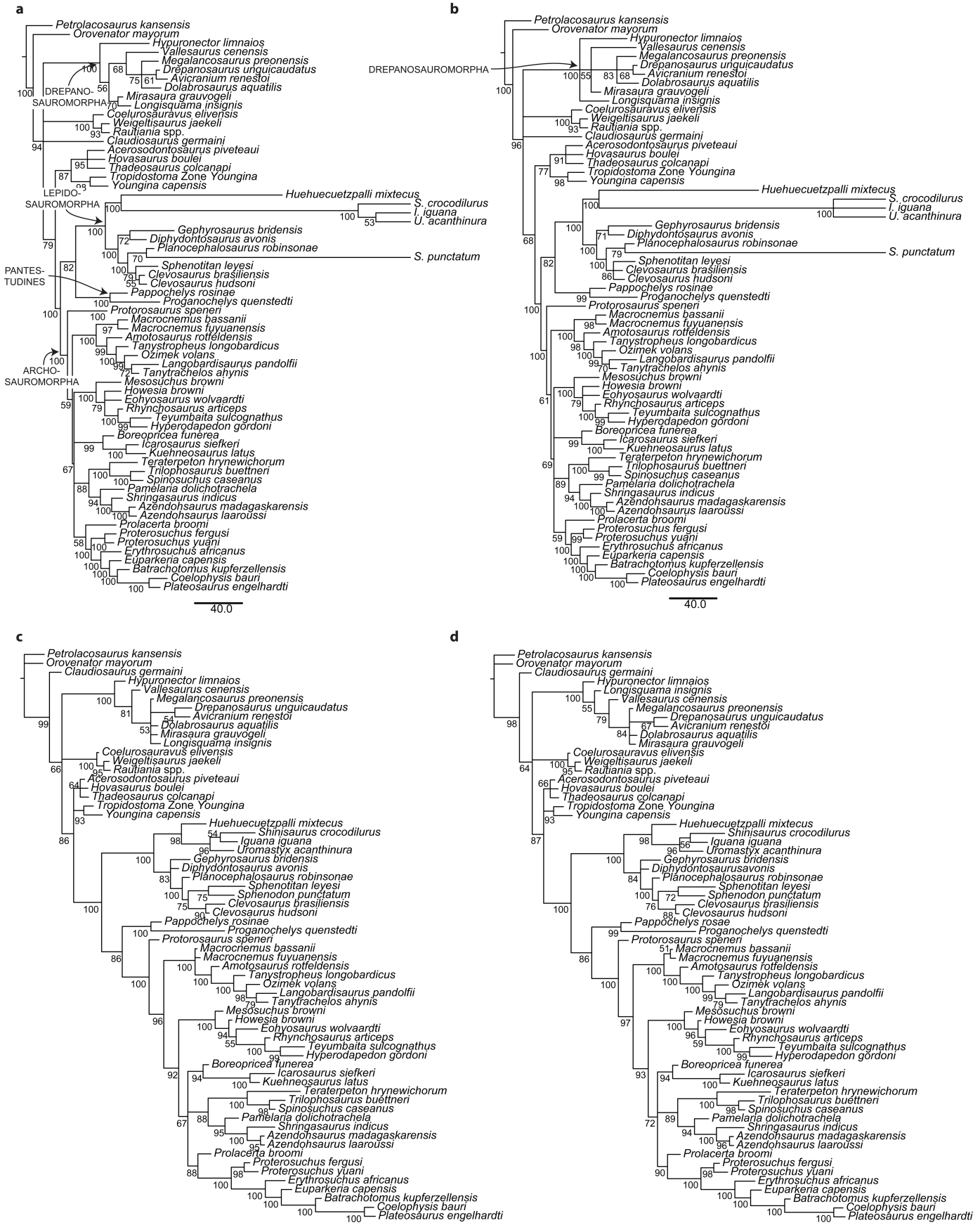

Extended Data Fig. 10 | Bayesian inference analyses results. a, Time-calibrated majority rule consensus tree including character 340 after 3,365,000 generations (when average standard deviation of split frequencies decreased below 0.01). **b**, Time-calibrated majority rule consensus tree excluding character 340 after 4,590,000 generations. **c**, Non-calibrated majority rule consensus tree including character 340 after 690,000 generations. **d**, Non-calibrated majority rule consensus tree excluding character 340 after 770,000 generations. Posterior probabilities are indicated below each node.

nature portfolio

Corresponding author(s): Stephan Spiekman

Last updated by author(s): Oct 14, 2024

Reporting Summary

Nature Portfolio wishes to improve the reproducibility of the work that we publish. This form provides structure for consistency and transparency in reporting. For further information on Nature Portfolio policies, see our Editorial Policies and the Editorial Policy Checklist.

Statistics

For all statistical analyses, confirm that the following items are present in the figure legend, table legend, main text, or Methods section.

n/a	Confirmed
☐	☒ The exact sample size (*n*) for each experimental group/condition, given as a discrete number and unit of measurement
☐	☒ A statement on whether measurements were taken from distinct samples or whether the same sample was measured repeatedly
☐	☒ The statistical test(s) used AND whether they are one- or two-sided *Only common tests should be described solely by name; describe more complex techniques in the Methods section.*
☐	☒ A description of all covariates tested
☐	☒ A description of any assumptions or corrections, such as tests of normality and adjustment for multiple comparisons
☒	☐ A full description of the statistical parameters including central tendency (e.g. means) or other basic estimates (e.g. regression coefficient) AND variation (e.g. standard deviation) or associated estimates of uncertainty (e.g. confidence intervals)
☐	☒ For null hypothesis testing, the test statistic (e.g. *F*, *t*, *r*) with confidence intervals, effect sizes, degrees of freedom and *P* value noted *Give P values as exact values whenever suitable.*
☐	☒ For Bayesian analysis, information on the choice of priors and Markov chain Monte Carlo settings
☒	☐ For hierarchical and complex designs, identification of the appropriate level for tests and full reporting of outcomes
☒	☐ Estimates of effect sizes (e.g. Cohen's *d*, Pearson's *r*), indicating how they were calculated

Our web collection on statistics for biologists contains articles on many of the points above.

Software and code

Policy information about availability of computer code

Data collection	CT acquisition: PyHST2 Melanosome geometry: ImageJ 1.54g
Data analysis	CT processing: Mimics Research v25.0, Blender 3.2 Phylogenetic analyses: TNT 1.6, MrBayes v3.2.7 Melanosome Geometry: RStudio v2023.12.1+402, packages: 'car', 'ggplot2' SRS-XRF: MicroAnalysis Toolkit v3.0.9

For manuscripts utilizing custom algorithms or software that are central to the research but not yet described in published literature, software must be made available to editors and reviewers. We strongly encourage code deposition in a community repository (e.g. GitHub). See the Nature Portfolio guidelines for submitting code & software for further information.

Data

Policy information about availability of data

All manuscripts must include a data availability statement. This statement should provide the following information, where applicable:

- Accession codes, unique identifiers, or web links for publicly available datasets
- A description of any restrictions on data availability
- For clinical datasets or third party data, please ensure that the statement adheres to our policy

Files related to the phylogenetic analyses and the analyses of melanosome geometry are available as Supplementary Files and at Figshare. The digital models and SRµCT data of the skull of SMNS 97278 are freely available at http://paleo.esrf.fr.

Research involving human participants, their data, or biological material

Policy information about studies with human participants or human data. See also policy information about sex, gender (identity/presentation), and sexual orientation and race, ethnicity and racism.

Reporting on sex and gender	n/a
Reporting on race, ethnicity, or other socially relevant groupings	n/a
Population characteristics	n/a
Recruitment	n/a
Ethics oversight	n/a

Note that full information on the approval of the study protocol must also be provided in the manuscript.

Field-specific reporting

Please select the one below that is the best fit for your research. If you are not sure, read the appropriate sections before making your selection.

☐ Life sciences ☐ Behavioural & social sciences ☒ Ecological, evolutionary & environmental sciences

For a reference copy of the document with all sections, see nature.com/documents/nr-reporting-summary-flat.pdf

Ecological, evolutionary & environmental sciences study design

All studies must disclose on these points even when the disclosure is negative.

Study description	Description of a new Triassic reptile preserving elongate integumentary appendages through 1) osteological description aided by PPC-SRµCT data and (UV) photography; 2) phylogenetic analyses to assess the position of the new taxon among reptiles; 3) investigation of integumentary appendages by studying melanosome geometry through SEM images and geochemical composition through SRS-XRF.
Research sample	All known specimens of Mirasaura grauvogeli, gen. et sp. nov., comprising two specimens preserving skeletal remains, and 80 further specimens preserving remains of integumentary appendages. For the phylogenetic and melanosome geometry analyses, previously published specimens or samples were used of relevant comparative taxa.
Sampling strategy	For phylogenetic analysis the most appropriate pre-existing dataset to establish the phylogenetic position of drepanosauromorphs among reptiles was used and expanded with relevant taxa (Mirasaura, Longisquama, and the stem-turtle Pappochelys and Proganochelys). For the melanosome geometry analysis small samples of only a few square mm were taken to maintain the integrity of the specimens, yet take a sufficiently large sample for statistical analyses of geometry.
Data collection	Initial sampling of soft tissues was conducted at the Staatliches Museum für Naturkunde Stuttgart by C. Gascó Martín, with small samples being taken from SMNS 97280, 97300, 97292, 97306, 97322, 97324, 97325, 97329, and 592 97341-97345. Further sampling of the particularly promising specimens SMNS 97310, SMNS 97280, and SMNS 97300 was conducted at University College Cork by V. Rossi and M. McNamara.
Timing and spatial scale	Sampling of soft tissues was conducted at the Staatliches Museum für Naturkunde Stuttgart in 2022. Upon identification of melanosomes, further sampling of particularly promising specimens and melanosome analysis was conducted at University College Cork in 2023 and 2024. Samples were kept purposely small (about 1 mm squared) to limit damage to the specimens.
Data exclusions	No data were excluded from the analyses.

Reproducibility	For both the phylogenetic and melanosome geometry analyses, all data are provided freely at FigShare to ensure reproducibility.
Randomization	Samples were taken from various parts of the integumentary appendage in various specimens. Particular sample locations were chosen to represent different anatomical regions and to reflect regions of particularly promising carbonaceous soft tissue preservation.
Blinding	Blinding was not relevant; no randomized control trials are included.

Did the study involve field work? ☐ Yes ☒ No

Reporting for specific materials, systems and methods

We require information from authors about some types of materials, experimental systems and methods used in many studies. Here, indicate whether each material, system or method listed is relevant to your study. If you are not sure if a list item applies to your research, read the appropriate section before selecting a response.

Materials & experimental systems

n/a	Involved in the study
☒	☐ Antibodies
☒	☐ Eukaryotic cell lines
☐	☒ Palaeontology and archaeology
☒	☐ Animals and other organisms
☒	☐ Clinical data
☒	☐ Dual use research of concern
☒	☐ Plants

Methods

n/a	Involved in the study
☒	☐ ChIP-seq
☒	☐ Flow cytometry
☒	☐ MRI-based neuroimaging

Palaeontology and Archaeology

Specimen provenance	The specimens of Mirasaura derive from several localities belonging to the Grès à Voltzia of the Vosges region of northeastern France, with the type specimen deriving from the locality at Cocheren. All specimens were collected by Louis Grauvogel during his excavations of the region between 1930 and 1978. The material remained in his private collection until this collection was donated to the Staatliches Museum für Naturkunde Stuttgart in Germany by Léa Grauvogel-Stamm (daughter of Louis Grauvogel) in 2019.
Specimen deposition	All studied specimens of Mirasaura are deposited at the Staatliches Museum für Naturkunde Stuttgart in Germany.
Dating methods	Dating of the specimens is based on the previously known age of the Grès à Voltzia (see Geological Context of Supplementary Information for more information).

☒ Tick this box to confirm that the raw and calibrated dates are available in the paper or in Supplementary Information.

Ethics oversight	No ethical approval was required. The specimens are reposited at a public institution and were donated to the Staatliches Museum für Naturkunde Stuttgart as part of the Grauvogel collection with approval of the French government.

Note that full information on the approval of the study protocol must also be provided in the manuscript.

Plants

Seed stocks	n/a
Novel plant genotypes	n/a
Authentication	n/a